

Non-global logs and clustering impact on jet mass with a jet veto distribution

Kamel Khelifa-Kerfa¹
School of Physics & Astronomy, University of Manchester,
Oxford Road, Manchester, M13 9PL, U.K.

Abstract

There has recently been much interest in analytical computations of jet mass distributions with and without vetos on additional jet activity [1–6]. An important issue affecting such calculations, particularly at next-to-leading logarithmic (NLL) accuracy, is that of non-global logarithms as well as logarithms induced by jet definition, as we pointed out in an earlier work [3]. In this paper, we extend our previous calculations by independently deriving the full jet-radius analytical form of non-global logarithms, in the anti- k_t jet algorithm. Employing the small-jet radius approximation, we also compute, at fixed-order, the effect of jet clustering on both C_F^2 and $C_F C_A$ colour channels. Our findings for the $C_F C_A$ channel confirm earlier analytical calculations of non-global logarithms in soft-collinear effective theory [5]. Moreover, all of our results, as well as those of [3], are compared to the output of the numerical program EVENT2. We find good agreement between analytical and numerical results both with and without final state clustering.

arXiv:1111.2016v3 [hep-ph] 14 Feb 2012

¹Kamel.Khelifa@hep.manchester.ac.uk

Contents

1	Introduction	1
2	Fixed-order calculations: $\mathcal{O}(\alpha_s)$	4
2.1	Observable and jet algorithms definitions	4
2.2	LO distribution	6
3	Fixed-order calculations: $\mathcal{O}(\alpha_s^2)$	7
3.1	τ_{E_0} distribution in the anti- k_t algorithm	8
3.1.1	C_F^2 term	8
3.1.2	$C_F C_A$ term and NGLs	8
3.2	τ_{E_0} distribution in the C-A algorithm	12
3.2.1	C_F^2 term	13
3.2.2	$C_F C_A$ term	15
4	Resummation of τ_{E_0} distribution	16
4.1	Resummation with anti- k_t algorithm	16
4.2	Resummation with C-A algorithm	18
5	Numerical results	19
6	Conclusion	24
A	Derivation of LO distribution	28
B	G_{nm} coefficients	30
C	Threshold thrust distribution in SCET	31
C.1	Resummation	32

1 Introduction

Event and jet shape variables have long served as excellent tools for testing QCD and improving the understanding of its properties (for a review, see [7]). Event/jet shape distributions have been used to extract some prominent parameters in QCD including the strong coupling and the quark–gluon colour ratio [8]. Due to the fact that shape variables are, by construction, linear in momentum, they exhibit a strong sensitivity to non-perturbative (NP) effects [7, 9]. They have thus been exploited to gain a better analytical insight into this QCD domain [7, 10]. Furthermore, jet shapes have been used not only to study the jet structure of hadronic final states, including jet multiplicities, jet rates and jet profiles (Ref. [11] and references therein), but also the *subset* structure, or substructure, of the jets themselves (for a recent example, see [1]). The latter subject has received significant attention in recent years, particularly in the area of boosted objects with the aim to separate the decay products of Beyond Standard Model (BSM) particles from QCD background at LHC (for a review, see [12]).

Although shape variables are, by construction, Infrared and Collinear (IRC) safe, fixed-order perturbative (PT) calculations break down in regions of phase space where the shape variable is small. These regions correspond to gluon emissions that are soft and/or collinear to hard legs and lead to the appearance of large logs that spoil the PT expansion of the shape distribution [11] (and references therein). While measured shape distributions have a peak near small values of the shape variable and then go to zero, fixed-order analytical distributions diverge. To deal away with these divergences and successfully reproduce the experimentally-seen behaviour, one ought to either perform an all-orders resummation of the large logs, matched to fixed-order result, or rely on Monte Carlo event generators. We are concerned, in the present paper, with the resummation method as it paves the way for a better understanding of QCD dynamics including the process of multiple gluon radiation. The general form of resummed distributions for observables that have the property of exponentiation can be cast as [11]

$$\Sigma(v) = C(\alpha_s) \exp [L g_1(\alpha_s L) + g_2(\alpha_s L) + \alpha_s g_3(\alpha_s L) + \dots] + D(v) \quad (1.1)$$

where $L = \ln(1/v)$, $C(\alpha_s)$ is an expansion in α_s with constant coefficients that can be inferred from fixed-order calculations and $D(v)$ collects terms that are proportional to powers of the shape variable v . The function g_1 resums all the leading logs (LL) $\alpha_s^n L^{n+1}$, while g_2 resums the next-to-leading logs (NLL) $\alpha_s^n L^n$ and so on.

There are two types of jet shape observables²: global and non-global [13]. *Global* observables are shape variables that are sufficiently inclusive over the whole final state phase space. The resummation of such variables, e.g, thrust, heavy jet mass and broadening, up to NLL accuracy have long been performed [14, 15]. The resultant resummed distributions were then matched with NLO fixed-order results for a better agreement with measurements over a wide range of values of the shape variable [14, 16]. In the recent past, the NNLL + NLO distribution has been obtained for energy-energy correlation [17], as well as NNLL + NNLO [18] for the thrust distribution [19], both in e^+e^- annihilation processes in QCD. Within the framework of Soft and Collinear Effective Theory (SCET) [20], the N³LL resummation for various event/jet variables have been performed [21] and used, after matching to NNLO, for a precise determination of the coupling constant α_s . The extracted value is consistent with the world average with significant improvements in the scale uncertainty.

At hadron colliders, what one often measures instead is jets, which only occupy patches of the phase space. The corresponding jet shape variables are thus non-inclusive, or non-global, and the resummation becomes highly non-trivial even at NLL level. Consider, for example, measuring the normalised invariant mass, ρ , of a subset of high- p_t jets in multijet events. A veto is applied on final state soft activity to keep the jet multiplicity fixed. Jets are only defined through a jet algorithm, which generally depends on some parameters such as the jet size R [22]. We are thus faced with a multi-scale (ρ , hard scale, veto, jet size) problem where potentially large logs in the ratios of these scales appear. In addition to the Sudakov leading logs, $\alpha_s^n \ln^{n+1} \rho$, coming from independent primary gluon emissions, there are large subleading non-global logs (NGLs) of the form $\alpha_s^n \ln^n(a/b)$, where a and b are two different scales, coming from secondary³ correlated gluon emissions.

²from the point of view of our calculations in this paper.

³These are emissions that are not radiated off primary hard legs.

We argued in [3] that in the narrow well-separated jets limit, the non-global structure of the ρ distribution, at hadronic colliders, becomes much like that of e^+e^- hemisphere jet mass [13]. This is mainly due to the fact that non-global logs arise predominantly near the boundaries of individual jets. We had therefore considered e^+e^- dijet events where only one of the jets is measured while the other is left unmeasured. We found, in the anti- k_t algorithm [23], NGLs in the ratio $\rho Q/2R^2 E_0$ as well as $2E_0/Q$ where E_0 and Q are the veto and hard scale respectively. These logs were completely missed out in [1,2]. The resummation of these NGLs to all-orders had been approximated to that of the hemisphere mass [13] up to terms vanishing as powers of R . Furthermore, we pointed out, by explicitly computing the jet mass (without jet veto) distribution under clustering, that different jet definitions differ at NLL due to clustering-induced large logs. Here we compute these logs, which we refer to as *clustering logs* (CLs), for the jet mass with a jet veto distribution.

Within the same context of e^+e^- multijet events, Kelley *et al.* [4] (version 1) proposed that if one measures the masses of the two highest-energy jets, instead of a single highest-energy jet as done in [3], then the resulting distribution is free from NGLs. This is clearly not correct since the latter shape observable, which we shall refer to, following [24], as *threshold thrust*⁴, is still non-global. To clearly see this consider, for example, the following gluonic configuration in e^+e^- dijet events at $\mathcal{O}(\alpha_s^2)$. A gluon k_1 is emitted by hard eikonal legs into the interjet energy region, Ω . k_1 then emits a softer gluon k_2 into, say the quark jet region. This configuration then contributes to the quark jet mass. The corresponding virtual correction, whereby gluon k_2 is virtual, does not, however, contribute to the quark jet mass. Hence, upon adding the two contributions one is left with a real-virtual mis-cancellation resulting in logarithmic enhancement of the jet mass distribution. The latter is what we refer to as NGLs. The other, antiquark, jet receives identical enhancement. Thus the sum of the invariant masses of the two jets does indeed contain NGLs contribution. The latter is actually twice that of the single jet mass found in [3].

Moreover, the authors of [4] (version 1) claimed that the anti- k_t [23] and Cambridge-Aachen (C-A) [25] jet algorithms only differ at NNLL for the threshold thrust⁵. From our calculation in [3] for the jet mass, which is not -with respect to clustering- much different from the threshold thrust, we know that the latter statement is incorrect. Nonetheless, an explicit proof will be presented below. Now, what is interesting in [4] and triggers the current work, is that the total differential threshold thrust distribution computed in the C-A algorithm and which contains neither NGLs nor CLs contributions, seemed to somehow agree well with next-to-leading (NLO) program **EVENT2** [26].

In this paper we shall shed some light on the result of [4] by considering the individual colour, C_F^2 , $C_F C_A$ and $C_F T_R n_f$, contributions to the total differential distribution as well as the effect of C-A clustering. We show that at $\mathcal{O}(\alpha_s^2)$ both NGLs and CLs are present and that the above agreement with **EVENT2** is, on one side merely accidental⁶, and on

⁴This name is more appropriate at hadron colliders where at threshold the final state jets are back-to-back and there is no beam remnant [24].

⁵This claim has been removed from version 2.

⁶As we shall see in sec. 5, while individual colour contributions do not agree with **EVENT2** their sum does, but only in the shape variable range and for the jet-radius considered in [4]. Outside the latter range or for other smaller jet-radii they do not agree.

the other side due to the fact that the interval of the threshold thrust considered in [4] does not correspond to the asymptotic region where large logs are expected to dominate. The current work may be regarded as an extension to [3]. It includes: (a) computing the full R dependence of the leading NGLs coefficient in the anti- k_t , (b) computing the small R approximation of the latter as well as the leading CLs coefficient in the C-A algorithm and (c) checking our findings, as well as those of [3], against EVENT2. It turns out, from the latter comparison, that the above approximation is actually valid for quite large values of R .

While the current paper was in preparation, a paper by Hornig *et al.* [5] appeared in arXiv which studied NGLs in various jet algorithms, including anti- k_t and C-A, within SCET. On the same day, Kelley *et al.* published version 2 of [4] in which they realised that this distribution is not actually free of NGLs and computed the corresponding coefficient in the anti- k_t algorithm. Our findings on NGLs, which were independently derived using a different approach to both papers, confirm the results of both SCET groups. Clustering effects on primary emission sector are unique to this paper.

The organisation of this paper is as follows. In sec. 2 we compute the full logarithmic part of the LO threshold thrust distribution. We then consider, in sec. 3, the fixed-order NLO distribution in the eikonal limit and compute the NGLs coefficient, in both anti- k_t and C-A jet algorithms. In the same section we derive an expression for the CLs' first term as well. Note that our calculations for the C-A algorithm are performed in the small R limit. Sec. 4 is devoted to LL resummation of our jet shape including an exponentiation of the NGLs' and CLs' fixed-order terms. The latter exponentiation suffices for our purpose in this paper, which is to compare the analytical distribution with EVENT2 at NLO. It also provides a rough estimate of the size and impact of NGLs and CLs on the total resummed distribution. In appendix C, the corresponding resummation in SCET [4,24,27] is presented. Numerical distributions of the threshold thrust obtained using the program EVENT2 are compared against analytical results and the findings discussed in sec. 5. In light of this discussion, we draw our main conclusions in sec. 6.

2 Fixed-order calculations: $\mathcal{O}(\alpha_s)$

After briefly reviewing the definition of the threshold thrust observable, or simply the jet mass with a jet veto, presented in [4,24], a general formula for sequential recombination jet algorithms is presented. We then move on to compute the LO integrated distribution of this shape variable. At this order, all jet algorithms are identical. Note that partons (quarks and gluons) are assumed on-mass shell throughout.

2.1 Observable and jet algorithms definitions

Consider e^+e^- annihilation into multijet events. First, cluster events into jets of size (radius) R with a jet algorithm. After clustering, label the momenta of the two hardest jets p_R and p_L and the energy of the third hardest jet E_3 . The threshold thrust is then given by the sum of the two leading jets' masses after events with $E_3 > E_0$ are vetoed [4],

$$\tau_{E_0} = \frac{m_R^2 + m_L^2}{Q^2} = \frac{\rho_R + \rho_L}{4}. \quad (2.1)$$

ρ_R and ρ_L are the jet mass fractions for the two leading jets respectively. We have shown in [3] that the single jet mass fraction, ρ , is a non-global shape variable. Thus τ_{E_0} must obviously be a non-global variable too.

A general form of sequential recombination algorithms at hadron colliders is presented in [22]. The adopted version for e^+e^- machines may be summarised as follows [22]: Starting with a list of final state pseudojets with momenta p_i ⁷, energies E_i and angles θ_i w.r.t. c.m frame, define the distances

$$d_{ij} = \min(E_i^{2p}, E_j^{2p}) \frac{2(1 - \cos \theta_{ij})}{R^2}, \quad d_{iB} = E_i^{2p}, \quad (2.2)$$

where p can be any (positive or negative) continuous number. At a given stage of clustering, if the smallest distance is d_{ij} then i and j are recombined together. Otherwise if the smallest distance is d_{iB} then i is declared as a jet and removed from the list of pseudojets. Repeat until no pseudojets are left. The recombination scheme we adopt here is the E -scheme, in which pairs (ij) are recombined by adding up their 4-momenta. Two pseudojets, i and j , are merged together if

$$2(1 - \cos \theta_{ij}) < R^2. \quad (2.3)$$

The anti- k_t , C-A and k_t algorithms correspond, respectively, to $p = -1, p = 0$ and $p = 1$ in eq. (2.2). We shall only consider the first two algorithms, anti- k_t and C-A in this paper. Calculations for the inclusive k_t are identical to those for the C-A algorithm as shown in [3]. With regard to notation, the jet-radius in [4], which we shall denote R_s , is given in terms of R by

$$R_s = R^2/4. \quad (2.4)$$

Here we work with R_s instead of R .

To verify that the definition (2.1) is just the thrust in the threshold (dijet) limit, hence the name, we begin with the general formula of the thrust,

$$\tau = 1 - \max_{\hat{\mathbf{n}}} \frac{\sum_i |\mathbf{p}_i \cdot \hat{\mathbf{n}}|}{\sum_i |\mathbf{p}_i|}, \quad (2.5)$$

where the sum is over all final state 3-momenta \mathbf{p} and the maximum is over directions (unit vectors) $\hat{\mathbf{n}}$. In the threshold limit, enforced by applying a veto on soft activity, e^+e^- annihilates into two back-to-back jets and the *thrust axis*, the maximum $\hat{\mathbf{n}}$, coincides with jet directions. At LO, an emission of a single gluon, k , that is collinear to, and hence clustered with say, p_R , produces the following contribution to the thrust

$$\tau \simeq \frac{E_R \omega}{Q} (1 - \cos \theta_{kp_R}) + \frac{E_L \omega}{Q} (1 - \cos \theta_{kp_L}) + \frac{\omega^2}{Q^2} (1 - \cos \theta_{kp_R})(1 - \cos \theta_{kp_L}), \quad (2.6)$$

where $E_{R(L)}$ is the energy of the hard leg $p_{R(L)}$, ω the gluon's energy and we have discarded an $\mathcal{O}(\tau^2)$ term. Recalling that the first two terms in the RHS of eq. (2.6) are just the mass fractions ρ_R and ρ_L , respectively, at LO and neglecting the third term (quadratic in ω) one concludes that

$$\tau \simeq \tau_{E_0}. \quad (2.7)$$

This relation can straightforwardly be shown to hold to all-orders.

⁷ p_i^μ may be the momenta of individual particles or each p_i^μ may be the total momentum of the particles whose paths are contained in a small cell of solid angle about the interaction point, as recorded in individual towers of a hadron calorimeter.

2.2 LO distribution

In [3] we computed the LO distribution of the jet mass fraction, ρ , in the small R (R_s) limit using the matrix–element squared in the eikonal approximation. In this section, we use the full QCD matrix–element to restore the complete R_s dependence of the singular part of the τ_{E_0} distribution. The general expression for the integrated and normalised τ_{E_0} distribution, or equivalently the τ_{E_0} shape fraction, is given by

$$\Sigma(\tau_{E_0}, E_0) = \int_0^{\tau_{E_0}} d\tau'_{E_0} \int_0^{E_0} dE_3 \frac{1}{\sigma} \frac{d^2\sigma}{d\tau'_{E_0} dE_3}, \quad (2.8)$$

where σ is the total $e^+e^- \rightarrow$ hadrons cross–section. The perturbative expansion of the shape fraction Σ in terms of QCD coupling α_s may be cast in the form

$$\Sigma = \Sigma^{(0)} + \Sigma^{(1)} + \Sigma^{(2)} + \dots, \quad (2.9)$$

where $\Sigma^{(0)}$ refers to the Born contribution and is equal to 1. The derivation of the first order correction, $\Sigma^{(1)}$, to the Born approximation is presented in appendix A. The final result reads

$$\begin{aligned} \Sigma^{(1)}(\tau_{E_0}, E_0) = & \frac{C_F\alpha_s}{2\pi} \left[-2\ln^2\tau_{E_0} + \left(-3 + 4\ln\frac{R_s}{1-R_s} \right) \ln\tau_{E_0} \right] \Theta\left(\frac{R_s}{1+R_s} - \tau_{E_0}\right) + \\ & + \frac{C_F\alpha_s}{2\pi} \left[-1 + \frac{\pi^2}{3} - 4\ln\frac{R_s}{1-R_s} \ln\frac{2E_0}{Q} + f_{E_0}(R_s) \right], \end{aligned} \quad (2.10)$$

where we have used eq. (A.2) to change the normalisation in eq. (2.8) from σ to σ_0 . The reason for this change is that the matrix–element we have used in EVENT2 is normalised to the Born cross–section⁸. The only difference between the two normalisations at $\mathcal{O}(\alpha_s)$ is in the one–loop constant. If we normalised to σ we would have found $C_F(-5/2 + \pi^2/3)$ instead of $C_F(-1 + \pi^2/3)$. The function $f_{E_0}(R_s)$ is given by

$$f_{E_0}(R_s) = -2\ln R_s \ln\frac{R_s}{1-R_s} + 2\text{Li}_2(R_s) - 2\text{Li}_2(1-R_s) + \frac{8E_0}{Q} \ln\frac{R_s}{1-R_s} + \mathcal{O}\left(\frac{E_0^2}{Q^2}\right). \quad (2.11)$$

Notice that eqs. (2.10) and (2.11) are identical to eqs. (1) and (2) of [4] v1 and the sum of the α_s parts of eqs. (65) and (66) in [5] provided that the jet radius in the latter, which we refer to as \bar{R} , is related to R_s by: $\tan^2(\bar{R}/2) = R_s/(1-R_s)$. It is worthwhile to note that in the limit $R_s \rightarrow 1/2$ the τ_{E_0} distribution (2.10) reduces to the well known thrust distribution [28] with upper limit $\tau < 1/3$. For $R_s < 1/2$ the threshold thrust distribution includes, in addition to thrust distribution, the interjet energy flow distribution [29] too,

$$\Sigma_{\text{E flow}}^{(1)}(E_0) = \frac{C_F\alpha_s}{2\pi} \left[-4\ln\frac{R_s}{1-R_s} \ln\left(\frac{2E_0}{Q}\right) + \mathcal{O}\left(\frac{E_0}{Q}\right) \right], \quad (2.12)$$

Here the interjet region (rapidity gap), referred to in literature as $\Delta\eta$, is defined by the edges of the jets. Specifically, it is related to the jet–radius R_s by

$$\Delta\eta = -\ln\left(\frac{R_s}{1-R_s}\right). \quad (2.13)$$

⁸Note that there are three sets of matrix–elements included in the program, of which only one is not normalised to the Born cross–section.

The important features of the τ_{E_0} distribution that are of concern to the present paper are actually contained in the second order correction term $\Sigma^{(2)}$, which we address in the next section.

3 Fixed-order calculations: $\mathcal{O}(\alpha_s^2)$

We begin this section by recalling the formula of the matrix-element squared for the e^+e^- annihilation into two gluons, $e^+e^- \rightarrow q(p_a) + \bar{q}(p_b) + g_1(k_1) + g_2(k_2)$ in the eikonal approximation. Let us first define the final state partons' 4-momenta as

$$\begin{aligned} p_a &= \frac{Q}{2}(1, 0, 0, 1), \\ p_b &= \frac{Q}{2}(1, 0, 0, -1), \\ k_1 &= \omega_1(1, \sin \theta_1 \cos \phi_1, \sin \theta_1 \sin \phi_1, \cos \theta_1), \\ k_2 &= \omega_2(1, \sin \theta_2 \cos \phi_2, \sin \theta_2 \sin \phi_2, \cos \theta_2). \end{aligned} \tag{3.1}$$

where the angles θ_i are w.r.t. p_a direction (which lies along the z -axis) and we assume the energies to be strongly ordered: $Q \gg \omega_1 \gg \omega_2$. This is so that one can straightforwardly extract the leading NGLs. Contributions from gluons with energies of the same order, $Q \gg \omega_1 \sim \omega_2$, are subleading and hence beyond our control. The recoil effects are negligible in the former regime and are thus ignored throughout. The eikonal amplitude reads [11],

$$S_{ab}(k_1, k_2) = C_F^2 W_P + C_F C_A W_S, \tag{3.2}$$

where W_P and W_S stand for primary and secondary emission amplitudes respectively. If we define the antenna function $w_{ij}(k) = 2(ij)/(ik)(kj)$ then the latter amplitudes are given by

$$W_P = w_{ab}(k_1)w_{ab}(k_2) = \frac{16}{\omega_1^2 \omega_2^2 \sin^2 \theta_1 \sin^2 \theta_2}, \tag{3.3}$$

and

$$\begin{aligned} W_S &= \frac{w_{ab}(k_1)}{2} [w_{a1}(k_2) + w_{b1}(k_2) - w_{ab}(k_2)], \\ &= \frac{8}{\omega_1^2 \omega_2^2 \sin^2 \theta_1 \sin^2 \theta_2} \left[\frac{1 - \cos \theta_1 \cos \theta_2}{1 - \cos \theta_{12}} - 1 \right], \end{aligned} \tag{3.4}$$

For completeness, the two-parton phase space is given by

$$d\Phi_2(k_1, k_2) = \left[\prod_{i=1}^2 \omega_i d\omega_i \frac{\sin \theta_i d\theta_i d\phi_i}{2\pi} \right] \left(\frac{\alpha_s}{2\pi} \right)^2, \tag{3.5}$$

It is worth noting that the primary emission, W_P , contribution to the τ_{E_0} distribution is only fully accounted for by the single-gluon exponentiation in the anti- k_t algorithm case. If the final state is clustered with a jet algorithm other than the latter, W_p integration over the modified phase space, due to clustering, leads to (see below) new logarithmic terms that escape the naive single-gluon exponentiation. On the other hand, the secondary

amplitude W_S contribution is completely missing from the latter Sudakov exponentiation in both algorithms.

First we outline the full α_s^2 structure of the τ_{E_0} distribution up to NLL level in the anti- k_t including the computation of the NGLs coefficient. After that, we investigate the effects of final state partons' clustering on both primary and secondary emissions. The C-A algorithm is taken as a case study to illustrate the main points. Calculations where the final state is clustered with other jet algorithms should proceed in an analogous way to the C-A case.

3.1 τ_{E_0} distribution in the anti- k_t algorithm

The anti- k_t jet algorithm works, in the soft limit, like a perfect cone. That is, a soft gluon k_i is clustered to a hard parton p_j if it is within an angular distance $2\sqrt{R_s}$ ($= R$), from the axis defined by the momentum of the latter. This feature of the algorithm greatly simplifies both fixed-order and resummation calculations. Considering all possible angular distances between (k_1, k_2) and (p_a, p_b) we compute below the corresponding contributions to primary and secondary pieces of the τ_{E_0} distribution. Note that we use LL and NLL to refer to leading and next-to-leading logs of τ_{E_0} (and not $2E_0/Q$) in the exponent of the resummed distribution (discussed in sec. 4).

3.1.1 C_F^2 term

The LL contribution to the τ_{E_0} distribution comes from diagrams corresponding to two-jet final states. That is diagrams where both real gluons, k_1 and k_2 , are clustered with the hard partons p_a and p_b . Diagrams where one of the two gluons is in the interjet region, and hence not clustered with either hard parton, contribute at NLL level. Other gluonic configurations lead to contributions that are beyond our NLL control and thus not considered. The C_F^2 part of the $\mathcal{O}(\alpha_s^2)$ τ_{E_0} distribution may be found by expanding the exponential of the LO result (2.10). The full expression including the running coupling at two-loop in the $\overline{\text{MS}}$ will be presented in sec. 4. For the sake of comparison to the clustering case, we only report here the the LL term, which reads

$$\Sigma_P^{(2)}(\tau_{E_0}, E_0) = 2 C_F^2 \left(\frac{\alpha_s}{2\pi} \right)^2 \ln^4(\tau_{E_0}). \quad (3.6)$$

Next we consider the derivation of the $C_F C_A$ contribution to the τ_{E_0} distribution including the full jet-radius dependence.

3.1.2 $C_F C_A$ term and NGLs

In the anti- k_t algorithm the non-global logarithmic contribution to the τ_{E_0} distribution is simply the sum of that of the single jet mass fraction, ρ , with a jet veto distribution studied in [3]⁹. This is in line with the near-edge nature of non-global enhancements. In two-jet events, the well separated¹⁰ jets receive the latter enhancements independently of each other. Possible final state gluonic arrangements relevant to NGLs at second order

⁹Here we go beyond the small R_s approximation assumed in [3].

¹⁰such that the jet-radius is much smaller than the jets' separation; $R_s \ll (1 - \cos\theta_{ij})$, where θ_{ij} is the angle between jets i and j .

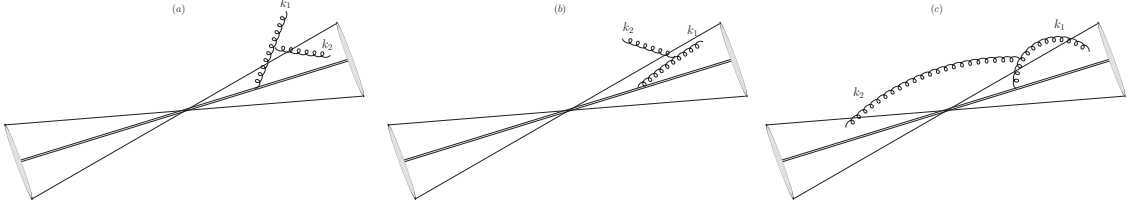


Figure 1: Schematic representation of gluonic arrangement giving rise to NGLs. We have only shown the NGLs contributions to the p_R -jet. Identical contributions apply to the p_L -jet.

are depicted in fig. 1. The all-orders resummed NGLs distribution may be written in the form [13]

$$S(t) = 1 + S_2 t^2 + \dots = 1 + \sum_{n=2} S_n t^n, \quad (3.7)$$

with t being the evolution parameter defined in terms of the coupling α_s by

$$\begin{aligned} t &= \frac{1}{2\pi} \int_{k_t^{\min}}^{k_t^{\max}} \frac{dk_t}{k_t} \alpha_s(k_t), \\ &= \frac{\alpha_s}{2\pi} \ln \left(\frac{k_t^{\max}}{k_t^{\min}} \right), \end{aligned} \quad (3.8)$$

where the exact form of the upper and lower limits, k_t^{\max} and k_t^{\min} , depend on the gluonic configuration and the second line in (3.8) assumes a fixed coupling. To make contact with interjet energy flow calculations [30, 31], we work in this particular section with hadronic variables (k_t, η, ϕ) instead of e^+e^- variables (E, θ, ϕ) . The pseudo-rapidity η and transverse momentum k_t (both measured w.r.t. incoming beam direction) are related, respectively, to the angle and energy by ¹¹

$$\eta = -\ln \left(\tan \frac{\theta}{2} \right), \quad E = k_t \cosh(\eta) \quad (3.9)$$

Using the secondary emissions eikonal amplitude (3.4) in terms of the new variables, the NGLs coefficient S_2 reads

$$S_2 = -4C_F C_A \int d\Phi^{(2)} \left[\frac{\cosh(\eta_1 - \eta_2)}{\cosh(\eta_1 - \eta_2) - \cos(\phi_1 - \phi_2)} - 1 \right], \quad (3.10)$$

where the phase space measure, $d\Phi^{(2)}$, is of the general form given in eq. (3.5) with the k_t integrals included in the definition of t (3.8) and new restrictions coming from the jet shape definition. For configuration (a) in fig. 1, it reads

$$d\Phi_a^{(2)} = \int_{-\frac{\Delta\eta}{2}}^{\frac{\Delta\eta}{2}} d\eta_1 \frac{d\phi_1}{2\pi} \times 2 \int_{\frac{\Delta\eta}{2}}^{+\infty} d\eta_2 \frac{d\phi_2}{2\pi} \Theta \left(\ln \frac{k_{t2}}{Q_{TE_0}} - \eta_2 \right) \Theta (E_0 - k_{t1} \cosh(\eta_1)), \quad (3.11)$$

¹¹Otherwise, one can redefine the partons' 4-momenta in terms of η and k_t and use the antenna function expressions of W_P and W_S to rewrite them in terms of the hadronic variables.

where the interjet (gap) region, $\Delta\eta$ is given in eq. (2.13). Due to boost invariance of rapidity variables the latter region has been centred at $\eta = 0$. Moreover, the factor 2 in (3.11) accounts for the p_L -jet contribution. Since neither the integrand nor the integral measure in eq. (3.10) depends explicitly on the azimuthal angles (ϕ_1, ϕ_2), we use our freedom to set $\phi_1 = 0$, average over ϕ_2 and then perform the rapidity integration. The resultant expression for S_2 in configuration (a) at the limit $\tau_{E_0} \rightarrow 0$ reads,

$$S_{2,a} = -4C_F C_A \left[\frac{\pi^2}{12} + \Delta\eta^2 - \Delta\eta \ln(e^{2\Delta\eta} - 1) - \frac{1}{2} \text{Li}_2(e^{-2\Delta\eta}) - \frac{1}{2} \text{Li}_2(1 - e^{2\Delta\eta}) \right] \quad (3.12)$$

An identical expression was found for the NGLs' coefficient in the interjet energy flow distribution [30]¹². The fact that $S_{2,a}$ is the same for τ_{E_0} and interjet energy flow distributions means that the NGLs' coefficient only depends on the geometry of the phase space and not on the observable itself. This is of course only true in the limit where the jet shape variable goes to zero. The difference between the jet shape variables amounts only to a difference in the logarithm's argument.

It should be understood that there are Θ -function constraints on k_{t1} and k_{t2} resulting from rapidity integrations not explicitly shown in eq. (3.12). Performing the remaining trivial k_t integrals yields

$$t_a^2 = \left(\frac{\alpha_s}{2\pi}\right)^2 \ln^2\left(\frac{2E_0 R_s}{Q\tau_{E_0}}\right) \Theta\left(\frac{2E_0}{Q} - \frac{\tau_{E_0}}{R_s}\right), \quad (3.13)$$

where a factor of 1/2 has been absorbed in $S_{2,a}$ (3.12).

Now consider configuration (b) in fig. 1. Adding up the corresponding virtual correction, one obtains the following phase space constraint

$$\Theta\left(\eta_1 - \ln\left(\frac{k_{t1}}{Q\tau_{E_0}}\right)\right) \Theta\left(k_{t2} - \frac{E_0}{\cosh(\eta_2)}\right). \quad (3.14)$$

The phase space measure $d\Phi_b^{(2)}$ is analogous to $d\Phi_a^{(2)}$ in (3.11) with $1 \leftrightarrow 2$ and the two Θ -functions in (3.11) replaced by those in eq. (3.14). The limits on η_1 are then $+\infty > \eta_1 > \max[\Delta\eta/2, \ln(k_{t1}/Q\tau_{E_0})]$. If we impose the constraint given in eq. (3.13), i.e. $2E_0/Q \gg \tau_{E_0}/R_s$, then the lower limit becomes $\eta_1 > \ln(k_{t1}/Q\tau_{E_0})$. The NGLs coefficient $S_{2,b}$ thus reads

$$S_{2,b} = -4C_F C_A \int_{\ln\frac{k_{t1}}{Q\tau_{E_0}}}^{+\infty} d\eta_1 \int_{-\frac{\Delta\eta}{2}}^{\frac{\Delta\eta}{2}} d\eta_2 [\coth(\eta_1 - \eta_2) - 1], \quad (3.15)$$

where we have averaged the eikonal amplitude W_s over ϕ_2 and moved k_{t1} 's Θ -functions onto the integral of the evolution parameter t_b , which is given at α_s^2 by

$$t_b^2 = \left(\frac{\alpha_s}{2\pi}\right)^2 \ln^2\left(\frac{2E_0}{Q}\right) \Theta\left(\frac{2E_0}{Q} - \frac{\tau_{E_0}}{R_s}\right). \quad (3.16)$$

The $S_{2,b} t_b^2$ contribution is then beyond our NLL accuracy. In fact, $S_{2,b}$ vanishes in the limit $\tau_{E_0} \rightarrow 0$ as can be seen from eq. (3.15).

¹²Our jet-radius, R_s , is given in terms the parameter c , used in [30], by the relation: $1 - c = 2R_s$.

The last contribution to NGLs at $\mathcal{O}(\alpha_s^2)$ comes from configuration (c) in fig. 1. Upon the addition of the virtual correction, one is left with the constraint

$$\Theta(Q\tau_{E_0} - k_{t1}e^{-\eta_1}) \Theta(k_{t2}e^{+\eta_2} - Q\tau_{E_0}). \quad (3.17)$$

The corresponding NGLs coefficient and evolution parameter read

$$S_{2,c} = -4C_F C_A \int_{\max\left[\ln\frac{k_{t1}}{Q\tau_{E_0}}, \frac{\Delta\eta}{2}\right]}^{+\infty} d\eta_1 \int_{-\ln\frac{k_{t2}}{Q\tau_{E_0}}}^{-\frac{\Delta\eta}{2}} d\eta_2 [\coth(\eta_1 - \eta_2) - 1], \quad (3.18)$$

$$t_c^2 = \left(\frac{\alpha_s}{2\pi}\right)^2 \ln^2(\tau_{E_0} e^{\Delta\eta/2}), \quad (3.19)$$

Since we have assumed strong ordering, $k_{t1} \gg k_{t2}$, then the lower limit of η_1 in (3.18) is $\ln(k_{t1}/Q\tau_{E_0})$. Consequently the coefficient $S_{2,c}$ vanishes in the limit $\tau_{E_0} \rightarrow 0$. For this reason, this configuration will not be considered.

We conclude that in the regime $2E_0/Q \gg \tau_{E_0}/R_s$, the only non-vanishing contribution to the NGLs comes from the phase space configuration (a). Other configurations, (b) and (c), vanish in the limit $\tau_{E_0} \rightarrow 0$. Hence

$$S_2 = S_{2,a}, \quad t = t_a. \quad (3.20)$$

In fig. 4 we plot S_2 as a function of the jet-radius R_s . At the asymptotic limit $\Delta\eta \rightarrow +\infty$ (or equivalently $R_s \rightarrow 0$) S_2 saturates at $-C_F C_A 2\pi^2/3$. This value (or rather half of it) is used as an approximation to S_2 in [3]. From eq. (3.12), we can see that the correction to such an approximation is less than 10% for jet-radii smaller than $R_s \sim 0.28$, which is equivalent to $R \sim 1$. Furthermore, Eq. (3.12) confirms the claim made in the same paper that NGLs do not get eliminated when the jet-radius approaches zero. One may naively expect that when the jet size shrinks down to 0 ($R_s \rightarrow 0$) there is no room for gluon k_2 to be emitted into. This means that τ_{E_0} becomes inclusive and hence S_2 vanishes. To the contrary, S_2 reaches its maximum in this limit.

Few important points to note:

- If we choose to order the energy scales in the Θ -functions of (3.13) and (3.16) the opposite way, i.e. $2E_0/Q \ll \tau_{E_0}/R_s$ then configuration (b) becomes leading, in NGLs, while the contribution from configuration (a) vanishes. That is t_b^2 in eq. (3.16) becomes

$$t_b^2 = \left(\frac{\alpha_s}{2\pi}\right)^2 \ln^2\left(\frac{2E_0 R_s}{Q\tau_{E_0}}\right) \Theta\left(\frac{\tau_{E_0}}{R_s} - \frac{2E_0}{Q}\right). \quad (3.21)$$

and $S_{2,b} = S_{2,a}$ in eq. (3.12). We do not consider this regime here though.

- If, on the other hand, we do not restrict ourselves to any particular ordering of the scales, as it is done in Refs. [5] and [4], then both configurations (a) and (b) would contribute to the leading NGLs. Adding up t_a^2 , in (3.13), and t_b^2 , in (3.21), the Θ -functions sum up to unity and one recovers the result reported in the above mentioned references. Notice that it is a straightforward exercise to show that eq. (3.12) is equal to $f_{OL} + f_{OR}$ given in eq. (28) of [5] in the case where $R_L = R_R = R$ ($= \bar{R}$ given in sec. 2). Moreover, the coefficient f_{NGL}^A given in eq. (B2) of [4] v2 is related to $S_{2,a}$ by $f_{\text{NGL}}^A = -8 \times S_{2,a}$.

- Setting the cut-off scale $E_0 \sim \tau_{E_0} Q$ in t_a , eq. (3.13), and t_b , eq. (3.21), would diminish NGLs coming from both configurations (a) and (b) and the threshold thrust becomes essentially a global observable. This is unlike the observation made in the study of the single jet with a jet veto distribution [3] where the above choice of E_0 kills the NGLs near the measured jet but introduces other equally significant NGLs near the unmeasured jet.

In the next subsection we recompute both C_F^2 and $C_F C_A$ contributions to the τ_{E_0} distribution under the C–A clustering condition. For the $C_F C_A$ term, we only focus on configuration (a) and do not attempt to address the subleading contributions coming from configurations (b) and (c).

3.2 τ_{E_0} distribution in the C–A algorithm

The definition of the C–A algorithm is given in eq. (2.2) with $p = 0$. Unlike the anti- k_t algorithm, which successively merges soft gluons with the nearest hard parton, the C–A algorithm proceeds by successively clustering soft gluons amongst themselves. Consequently, a soft parton may in many occasions be dragged into (away from) a jet region and hence contributing (not contributing) to the invariant mass of the latter. The jet mass, and hence τ_{E_0} , distribution is then modified. It is these modifications, due to soft-gluons self-clustering, that we shall address below.

Any clustering-induced contribution to the τ_{E_0} distribution will only arise from phase space configurations where the two soft gluons, k_1 and k_2 , are initially (that is, before applying the clustering) in different regions of phase space. Configurations where both gluons are within the same jet region, gluon k_1 is in one of the two jet regions and gluon k_2 is in the other or both gluons are within the interjet region are not altered by clustering and calculations of the corresponding contributions will yield identical results to the anti- k_t algorithm. We can therefore write the τ_{E_0} distribution in the C–A algorithm, at $\mathcal{O}(\alpha_s^2)$, as

$$\Sigma_{C-A}^{(2)}(\tau_{E_0}, E_0) = \Sigma_{\text{anti-}k_t}^{(2)}(\tau_{E_0}, E_0) + \delta\Sigma^{(2)}(\tau_{E_0}, E_0). \quad (3.22)$$

It is the last term in eq. (3.22) that we compute in the present subsection. Starting at configurations with two gluons in two different regions, the jet algorithm either:

- (A) recombines the two soft gluons into a single parent gluon if the clustering condition (2.3) is satisfied. The latter parent gluon will either be in one of the two jet regions or out of both of them (and hence in the interjet region).
- (B) or leaves the two gluons unclustered, if the clustering condition is not satisfied. This case is then identical to the anti- k_t one but with a more restricted phase space. This restriction comes from the fact that for the two gluons to survive the clustering they need to be sufficiently far apart. Quantitatively, their angular separation should satisfy the relation

$$(1 - \cos \theta_{12}) > 2R_s. \quad (3.23)$$

Below, we examine the contributions from configurations (A) and (B) to the C_F^2 and $C_F C_A$ colour pieces of the τ_{E_0} distributions. All calculations are performed in the small R_s approximation using the e^+e^- variables (ω, θ, ϕ) .

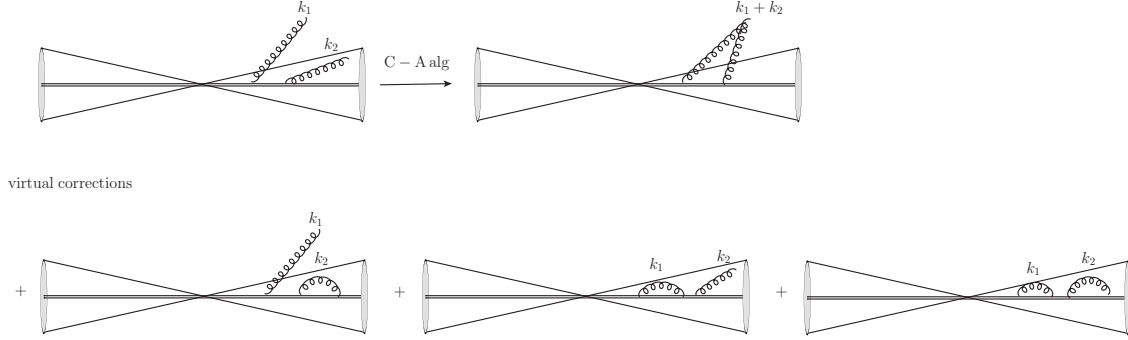


Figure 2: A schematic representation of a three-jet final state after applying the C-A algorithm on real emission along with virtual correction diagrams. The two gluons are clustered in the E-Scheme (see sec. 2). Identical diagrams hold for the p_L -jet.

3.2.1 C_F^2 term

Consider the gluonic configuration in (A) where the harder gluon k_1 is in the interjet region and the softer gluon k_2 is in the p_R -jet region. We account for the p_L -jet region through multiplying the final result by a factor of two. Applying the C-A algorithm (2.2), the smallest distance is $d_{\min} = d_{12}$. Hence gluon k_1 pulls gluon k_2 out of the p_R -jet region and form a third jet, as depicted in fig. 2. The latter is then vetoed to have energy less than E_0 . The corresponding clustering angular function, in the small angles limit, reads

$$\begin{aligned} \Theta_{\text{C-A}}(1, 2) &= \Theta(\theta_1^2 - 4R_s)\Theta(4R_s - \theta_2^2)\Theta(\theta_2^2 - \theta_{12}^2), \\ &= \Theta(4\theta_2^2 \cos^2 \phi_2 - \theta_1^2)\Theta(\theta_1^2 - 4R_s)\Theta(4R_s - \theta_2^2)\Theta\left(\theta_2^2 - \frac{R_s}{\cos^2 \phi_2}\right)\Theta\left(\cos \phi_2 - \frac{1}{2}\right). \end{aligned} \quad (3.24)$$

Adding up the corresponding virtual corrections, where one or both of the gluons are virtual, one obtains the following constraint on the phase space

$$\Theta(E_0 - \omega_1 - \omega_2) - \Theta(E_0 - \omega_1) + \Theta\left(\frac{\omega_2}{2Q}\theta_2^2 - \tau_{E_0}\right). \quad (3.25)$$

Since we are working in the strong energy-ordered regime, $\omega_1 \gg \omega_2$, only the last Θ -function survives. The new contribution to the C_F^2 piece of the τ_{E_0} distribution is then given by

$$\begin{aligned} C_2^P t_p^2 &= 8 \int_{\frac{Q\tau_{E_0}}{2R_s}}^{Q/2} \frac{d\omega_2}{\omega_2} \int_{\omega_2}^{Q/2} \frac{d\omega_1}{\omega_1} \int_{-\pi/3}^{\pi/3} \frac{d\phi_2}{2\pi} \int_{2\sqrt{R_s}}^{2\theta_2 \cos \phi_2} \frac{d\theta_1}{\theta_1} \int_{2\sqrt{R_s}}^{R_s/\cos \phi_2} \frac{d\theta_2}{\theta_2}, \\ &= 0.73 C_F^2 \left(\frac{\alpha_s}{2\pi}\right)^2 \ln^2\left(\frac{R_s}{\tau_{E_0}}\right). \end{aligned} \quad (3.26)$$

This result is identical to ¹³ that found in [3] for a single jet mass (without a jet veto) distribution. The reason for this is that the clustering requirement only affects the dis-

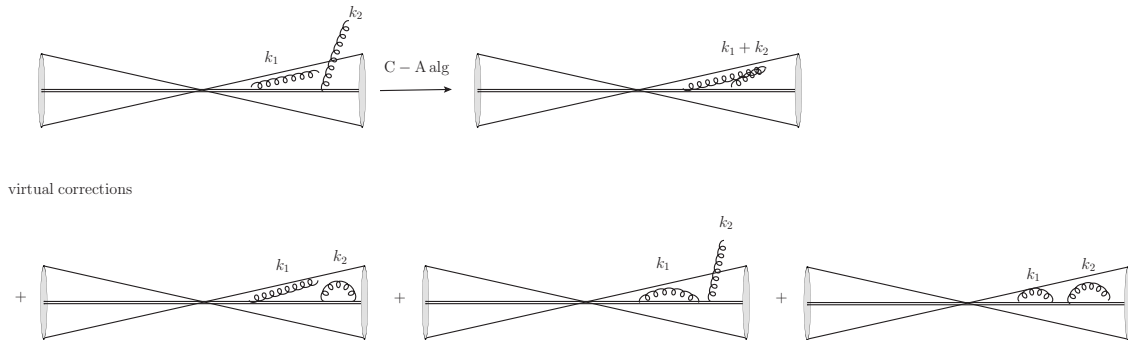


Figure 3: A schematic representation of a two-jet final state after applying the C–A algorithm on real emission along with virtual correction diagrams. The two gluons are clustered in the E–Scheme (see sec. 2). Identical diagrams hold for the left (p_L) jet.

tribution to which the softest gluon contributes. Which is in both cases the jet mass distribution.

The second possible configuration that corresponds to case (A) is where gluon k_1 is in, say, the p_R -jet region and the softer gluon k_2 is in the interjet region. If the two gluons are clustered, i.e, gluon k_1 pulls in gluon k_2 , then upon adding real emission and virtual correction diagrams, depicted in fig. 3, one obtains the following phase space constraint

$$-\Theta\left(\tau_{E_0} - \frac{\omega_1}{2Q}\theta_1^2\right)\Theta\left(\frac{\omega_2}{2Q}\theta_2^2 - \tau_{E_0}\right) + \Theta(\omega_2 - E_0), \quad (3.27)$$

where we have assumed small angles limit and employed the LL accurate approximation

$$\Theta\left(\tau_{E_0} - \frac{\omega_1}{2Q}\theta_1^2 - \frac{\omega_2}{2Q}\theta_2^2\right) \simeq \Theta\left(\tau_{E_0} - \frac{\omega_1}{2Q}\theta_1^2\right)\Theta\left(\tau_{E_0} - \frac{\omega_2}{2Q}\theta_2^2\right). \quad (3.28)$$

Given the fact that $\omega_1 \gg \omega_2$ and θ_1 and θ_2 must be close to each other to be clustered, i.e, they should satisfy condition (3.23), then the first two Θ -functions in eq. (3.27) are substantially suppressed and one is only left with the veto on ω_2 . Applying the C–A algorithm one obtains an identical clustering function to eq. (3.24). Hence the CLs' coefficient for this configuration is equal to C_2^P given in eq. (3.26). That is $C_2^P = 0.73 C_F^2$. The evolution parameter does however change. It is now given, at $\mathcal{O}(\alpha_s^2)$, by

$$t_p'^2 = \left(\frac{\alpha_s}{2\pi}\right)^2 \ln^2\left(\frac{2E_0}{Q}\right). \quad (3.29)$$

This contribution is then beyond our NLL control. Note that the CLs contribution in eq. (3.29) is equal to what one would find for interjet energy flow distribution provided that the rapidity gap is defined through eq. (2.13).

Let us now turn to case (B) where the two gluons are not merged together. If gluon k_1 is in the interjet region and gluon k_2 is in one of the two jet regions then the corresponding phase space constraint reads

$$\Theta\left(\frac{2Q\tau_{E_0}}{\omega_2} - \theta_2^2\right)\Theta(\omega_1 - E_0)[1 - \Theta_{C-A}(1, 2)]. \quad (3.30)$$

¹³It is actually twice

The limits on θ_2 -integral are then given by: $\min(4R_s, 2Q\tau_{E_0}/\omega_2) > \theta_2^2 > 0$. Imposing the constraint $2E_0/Q \gg \tau_{E_0}/R_s$, it is straightforward to see that the above constraint yields NNLL contribution and thus beyond our control. Similarly, the configuration where gluon k_1 is in the jet region and gluon k_2 is in the interjet region yields subleading logs.

Hence the C_F^2 piece of the clustering-induced correction term $\delta\Sigma^{(2)}$, in eq. (3.22), up to NLL, reads

$$\delta\Sigma^{(2)}(\tau_{E_0}, E_0) = C_2^P t_p^2, \quad (3.31)$$

Next we compute the $C_F C_A$ piece of $\delta\Sigma^{(2)}$.

3.2.2 $C_F C_A$ term

Consider the gluonic configuration (a) depicted in fig. 1. Applying the C–A clustering algorithm on the latter yields two possibilities. Namely the two gluons are either clustered or not. The former case completely cancels against virtual corrections and thus does not contribute to NGLs. It is when the two gluons survive the clustering, the latter case, that a real–virtual mismatch takes place and NGLs are induced. The corresponding evolution parameter is equal to t of the anti- k_t case, eq. (3.20). The clustering condition is simply one minus that in eq. (3.24). The NGLs' coefficient can then be written, using the eikonal amplitude (3.4), as

$$S_2^{C-A} = S_2 + \delta\Sigma_{C_F C_A}^{(2)} \quad (3.32)$$

where S_2 is given in eq. (3.20) and

$$\begin{aligned} \delta\Sigma_{C_F C_A}^{(2)} = 8 C_F C_A \int_{\sqrt{R_s}}^{2\theta_2 \cos \phi_2} \frac{d\theta_1}{\sin \theta_1} \int_{\frac{\sqrt{R_s}}{\cos \phi_2}}^{2\sqrt{R_s}} \frac{d\theta_2}{\sin \theta_2} \int_{-\pi/3}^{\pi/3} \frac{d\phi_2}{2\pi} \left[\frac{1 - \cos \theta_1 \cos \theta_2}{1 - \cos \theta_{12}} - 1 \right] \times \\ \times \Theta \left(\frac{R_s}{\tau_{E_0} \cos \phi_2} - \frac{Q}{2\omega_2} \right), \quad (3.33) \end{aligned}$$

We can perform the θ_1 -integral analytically and then resort to numerical methods to evaluate the remaining θ_2 and ϕ_2 integrals. The result, in terms of the jet-radius R_s , is depicted in Fig. 4. $-S_2^{C-A}$ saturates at around $0.44 \times 2\pi^2/3 C_F C_A \sim 2.92 C_F C_A$, i.e. a reduction of about 55% in S_2 . This is due to the fact that for the two gluons to survive clustering they need to be sufficiently far apart ($\theta_{12} > R = 2\sqrt{R_s}$). The dominant contribution to S_2 comes, however, from the region of phase space where the gluons are sufficiently close. This corresponds to the collinear region of the matrix-element; $\theta_1 \sim \theta_2$. Hence the further apart the two gluons get from each other, the less (collinear) singular the matrix becomes and thus the smaller the value of NGLs coefficient.

Note that the C–A coefficient $S_2^{C-A} = 2 \times f_{\text{OR}}^{C/A}$, where $f_{\text{OR}}^{C/A}$ is given by eq. (38) in [5], at least in the small jet-radius region. Noticeably, the two results coincide at both limits $R_s \rightarrow 0$ and $R_s \rightarrow 1/2$ (equivalently $R \rightarrow 0$ and $R \rightarrow \sqrt{2}$ in [5]). In fact, the coefficient S_2^{C-A} is valid, as we shall see in sec. 5, for quite large jet-radii; up to $R_s \sim 0.3$ (equivalent to $R \sim 1$ in [5]).

The fixed-order NLL logarithmic structure of the τ_{E_0} distribution should by now be clear for both jet algorithms. In order to assess the phenomenological impact of NGLs and clustering requirement on the final cross-section, it is necessary to perform an all-orders treatment, which we do below.

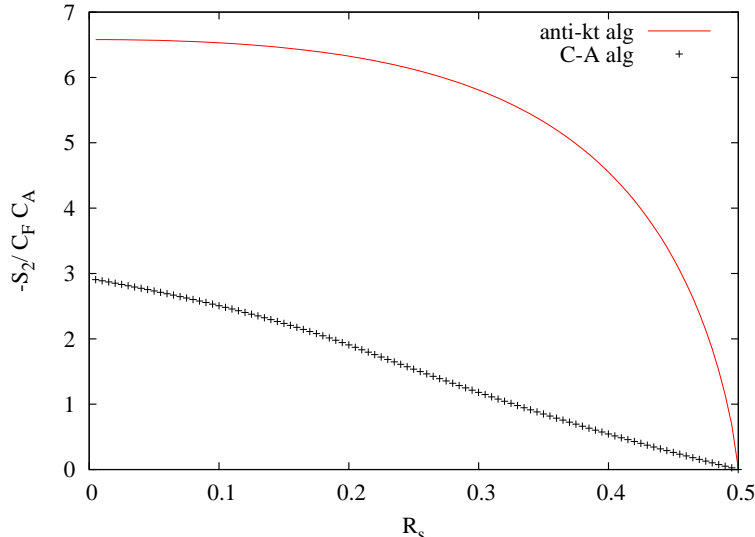


Figure 4: Non-global coefficient S_2 in the anti- k_t and C-A algorithms.

4 Resummation of τ_{E_0} distribution

Resummation, which is essentially the organisation of large logs arising from soft and/or collinear radiation to all-orders, is based on the factorisation property of the pQCD matrix-element squared for multiple gluon radiation. This is only true for independent primary emissions though. Including secondary correlated emissions, the picture dramatically changes and the resummation can only be performed at some limits, eg. large- N_c limit [32]. In the standard method [14, 33, 34], resummation is carried out in Mellin (Laplace) space instead of momentum space. Only at the end does one transform the result back to the momentum space through (inverse Mellin transform),

$$\Sigma_P(\tau_{E_0}, E_0) = \int \frac{d\nu}{2i\pi\nu} e^{\nu\tau_{E_0}} \int \frac{d\mu}{2i\pi\mu} e^{\mu E_0} \tilde{\Sigma}_P(\nu^{-1}, \mu^{-1}), \quad (4.1)$$

where P stands for primary emission. With regard to non-global observables, the important point to notice is that the resummation of NGLs is included as a factor multiplying the single-gluon Sudakov form factor, Σ_P , [13]

$$\Sigma(\tau_{E_0}, E_0) = \Sigma_P(\tau_{E_0}, E_0) S(t), \quad (4.2)$$

In this section, we first consider resummation of τ_{E_0} distribution in events where the final state jets are defined in the anti- k_t algorithm and, second, discuss the potential changes to the resummed result when the jets are defined in the C-A algorithm instead.

4.1 Resummation with anti- k_t algorithm

As stated in the introduction and proved in sec. 2, the τ_{E_0} observable is simply the sum of the invariant masses of the two highest-energy (or highest- p_t for hadron colliders) jets. Therefore the τ_{E_0} resummed Sudakov form factor is just double that computed in [3], for

a single jet mass. That is, up to NLL level we have

$$\Sigma_P(\tau_{E_0}, E_0) = \frac{\exp \left[-2 \left(\mathcal{R}_{\tau_{E_0}}(\tau_{E_0}) + \gamma_E \mathcal{R}'_{\tau_{E_0}}(\tau_{E_0}) \right) \right]}{\Gamma \left(1 + 2 \mathcal{R}'_{\tau_{E_0}}(\tau_{E_0}) \right)} \exp \left[-\mathcal{R}_{E_0}(E_0) \right]. \quad (4.3)$$

The full derivation of (4.3) as well as the resultant expressions of the various radiators are presented in the small jet-radius limit in Ref. [3]. To restore the full R_s dependence we make the replacement $R^2/\rho \mapsto R_s/(\tau_{E_0}(1 - R_s))$ such that when expanded eq. (4.3) reproduces at $\mathcal{O}(\alpha_s)$ the LO distribution (2.10).

To account for the NGLs at all-orders in α_s , it is necessary to consider an arbitrary ensemble of energy-ordered, soft wide-angle gluons that coherently radiate a softest gluon into the vetoed region of phase space [13]¹⁴. The analytical resummation of NGLs is then plagued with mathematical problems coming from geometric and colour structure of the gluon ensemble. Two methods have been developed to address this issue: A numerical Monte Carlo evaluation [13, 30] and a non-linear evolution equation that resums single logs (SL) at all-orders [35]. Both methods are only valid in the large- N_c limit. In the latter limit and for small values of the jet-radius R_s , we argued in [3] that the form of $S(t)$ should be identical to that found in the hemisphere jet mass case [13]. Since in the present paper we are not confined to the small R_s limit, we need to modify and re-run the Monte Carlo algorithm, presented in [13], for medium and large values of the jet-radius should we seek to resum the τ_{E_0} NGLs distribution. The latter task is, however, beyond the scope of this paper. Here, we are only aiming at comparing the analytical results with fixed-order NLO program `EVENT2`. It suffices in this case to simply exponentiate the first NGLs term in eq. (3.20),

$$S(t) = \exp \left(S_2 t^2 \right). \quad (4.4)$$

The distribution (4.2) is of the generic form given in eq. (1.1). Explicitly, it reads

$$\Sigma(\tau_{E_0}, E_0) = \left(1 + \sum_{k=1}^{\infty} C_k \left(\frac{\alpha_s}{2\pi} \right)^k \right) \exp \left[\sum_{n=1}^{\infty} \sum_{m=0}^{n+1} G_{nm} \left(\frac{\alpha_s}{2\pi} \right)^n \tilde{L}^m \right] + D_{\text{fin}}(\tau_{E_0}), \quad (4.5)$$

where C_k is the k^{th} loop-constant, $\tilde{L} = \ln(1/\tau_{E_0})$ and $D_{\text{fin}} \equiv D$, which vanishes in the limit $\tau_{E_0} \rightarrow 0$. In order to determine the coefficients G_{nm} at NLO and up to NLL, we need to expand the radiators, as well as the Γ function, in eq. (4.3) up to second order in the fixed coupling $\alpha_s = \alpha_s(Q)$. The results are presented in appendix. B. Although we have provided the NNLL coefficient, G_{21} in eq. (B.1), we do not claim that it is under control. Nonetheless, it does capture all R_s -dependent terms¹⁵. The missing terms from G_{21} include: a) coefficients of \tilde{L} which are independent of $\ln(R_s/(1 - R_s))$ for all colour channels. These can be borrowed from thrust distribution [19, 36, 37]. b) Although G_{21} has a subleading NGLs term in the $C_F C_A$ colour channel, which comes solely from the expansion of t (eq. (3.20)), the full expression in this channel as well as in the $C_F T_R n_f$

¹⁴In our case the vetoed region is the jet region. Due to symmetry, we can choose one jet region and multiply the final answer by a factor of two.

¹⁵as can be seen from comparison to the SCET result (C), which only contains the primary emission piece and is valid to NNLL.

channel is still missing. To properly compute the latter, one has to extend both the matrix-element (3.2) and the phase space to include hard emission. Such a task will be considered elsewhere. It is worthwhile to mention that full subleading NGLs have recently been computed analytically within SCET framework for the hemisphere mass variable [36, 37]¹⁶. The two-loop constant C_2 has also been computed for the latter variable as well as the thrust [19, 36].

To make contact with SCET calculations, we provide in appendix C the full formula of the Sudakov form factor for the τ_{E_0} primary distribution including determination of the G_{nm} coefficients in SCET.

Next we comment on the form of resummation when final state jets are defined in the C–A algorithm.

4.2 Resummation with C–A algorithm

With regard to primary emission piece, resumming logs induced by clustering is a cumbersome but doable task. It has been performed, for example, in [38] for interjet energy flow distribution where final state jets are defined in the inclusive k_t algorithm. The final result of the resummed radiator was written as an expansion in the jet-radius and the first four terms were determined. For secondary emissions, the resummation of NGLs has only been possible numerically and in the large- N_c limit. It has again been carried out for the above mentioned energy flow distribution in [31]. We expect that analogous, to the interjet energy flow, analytical treatment and numerical evaluation can be achieved for the resummation of CLs and NGLs, respectively, for the τ_{E_0} variable. We postpone this work to future publications.

For the sake of comparing to EVENT2, it is sufficient to simply exponentiate the fixed-order terms S_2^{C-A} and C_2^P , just as we did with the anti- k_t algorithm case. Due to the fact that logarithmic contributions induced by clustering arise mainly from soft wide-angle gluons, we expect them -clustering-induced logs- to factorise from the primary form factor at all-orders. Therefore, the resummed distribution, whereby clustering is imposed on the final state, may be written as

$$\Sigma(\tau_{E_0}, E_0) = \Sigma_P(\tau_{E_0}, E_0) S^{C-A}(t) C^P(t_p), \quad (4.6)$$

where S^{C-A} is of the form (4.4) with S_2 replaced by S_2^{C-A} and, in analogy with the NGLs factor, the CLs factor reads

$$C^P(t_p) = \exp(C_2^P t_p^2), \quad t_p = \int_{Q\tau_{E_0}/2R_s}^{Q/2} \frac{dk_t \alpha_s(k_t)}{k_t 2\pi}. \quad (4.7)$$

In fig. 5 we plot the resummed differential distributions, $d\Sigma(\tau_{E_0}, E_0)/d\tau_{E_0} = (1/\sigma_0)d\sigma/d\tau_{E_0}$, computed from eq. (4.3) for the anti- k_t algorithm and from eq. (4.6) for the C–A algorithm at different values of R_s . The dependence on E_0 has been discussed in [3] where the all-orders NGLs resummed expression was employed. There are several points to note. Firstly the effect of NGLs is a suppression of the total cross-section relative to the primary result. This suppression is diminished by decreasing the value of R_s . For example,

¹⁶Recall that for the leading NGLs the corresponding coefficient for the hemisphere mass distribution corresponds to setting $R_s = 0$ in $S_{2,a}$ (3.12).

at $E_0 = 0.1Q$ the Sudakov peak is reduced due to NGLs by about 4.02%, 3.42%, 2.62% and 1.35% for $R_s = 0.30, 0.12, 0.04$ and 0.0025 (equivalent to $R = 1.1, 0.7, 0.4$ and 0.1) respectively. These values are only meant to give an idea of the effect of varying the jet-radius parameter on both NGLs and CLs corrections to the total cross-section, since we are only working with an approximation of the latter and not the full all-orders result. It has been shown in [31], for the interjet energy distribution, that the NGLs resummed factor $S(t)$ at all-orders is much smaller (thus larger suppression of primary-only result) and of different shape, as a function of t , to the fixed-order exponentiated result.

Secondly the effect of clustering is reducing the phenomenological significance of NGLs. This reduction becomes larger, hence the NGLs suppression on the Sudakov peak becomes smaller, as one moves towards smaller values of R_s . For the same jet veto $E_0 = 0.1Q$, the Sudakov peak is reduced by 0.62%¹⁷, 0.80%, 0.63% and 0.22% for $R_s = 0.30, 0.12, 0.04$ and 0.0025 respectively (values are only an estimate of the impact of clustering). Comparing to the anti- k_t case, we see that the effect of NGLs has been reduced by more than 70% for $R_s = 0.12, 0.04$ and $R_s = 0.0025$. This observation suggests that instead of resumming NGLs, which is a daunting task even numerically, one should, perhaps, attempt at eliminating them at each order through requiring final state clustering and looking for the optimal value of the jet-radius, and may be the jet veto too, such that non-global corrections are wiped out. In our rough approximation, we find that NGLs are completely eliminated, leaving only the primary Sudakov form factor, at $R_s \lesssim 3 \times 10^{-5}$ (equivalent to $R \lesssim 0.01$). Although this value is very small and not of any practical significance, including the full all-orders resummed results for both NGLs and CLs might result in practically larger values. Whether this is indeed the case remains to be investigated. If it turns out that the optimal radius is relatively large, $0.04 \lesssim R_s$ ($0.4 \lesssim R$), then final state clustering will be the key to solve the NGLs subtlety of non-global observables.

In the next section, we compare our analytical calculations to **EVENT2**. In particular, we focus on establishing the presence of NGLs and CLs in the τ_{E_0} distribution at NLO.

5 Numerical results

The τ_{E_0} numerical distribution has been computed using the fixed-order NLO QCD program **EVENT2**. The program implements the Catani-Seymour subtraction formalism for NLO corrections to two- and three-jet events observables in e^+e^- annihilation. Final state partons have been clustered into jets using the **FastJet** library [39]. The latter provides an implementation of the longitudinally invariant k_t , Cambridge-Aachen (CA) and anti- k_t jet finders along with many others. Cone algorithms such as SISCone [40] are also implemented as plugins for the package. It should be noted that the e^+e^- version of the aforementioned algorithms employs the following clustering condition for a pair of partons (ij)

$$1 - \cos \theta_{ij} < 1 - \cos(\tilde{R}), \quad (5.1)$$

¹⁷The discrepancy at $R_s = 0.30$ is due to the fact that we have employed the small angles approximation in the C-A calculations.

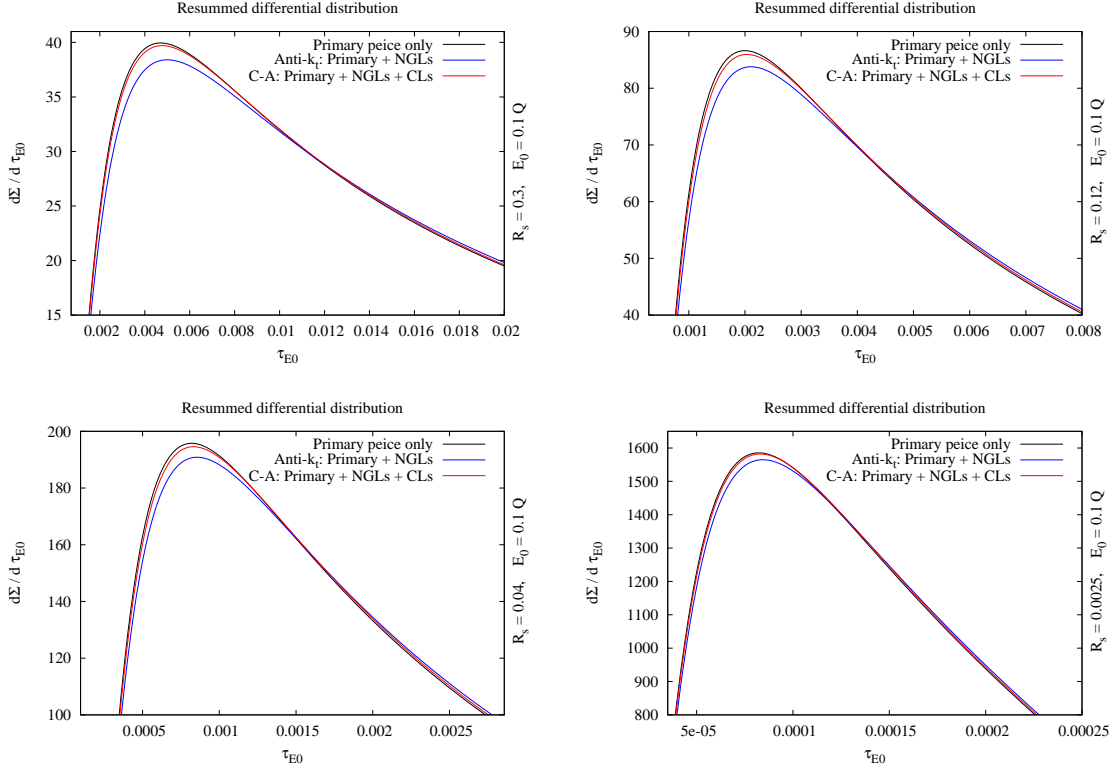


Figure 5: Comparison of analytical resummed differential distribution $d\Sigma/d\tau_{E_0}$ where: only primary term included (4.3), primary and NGLs factor included in the anti- k_t algorithm (4.3) and primary + NGLs + CLs factors included (4.6). The plots are shown for various jet-radii with a jet veto $E_0 = 0.1Q$. The coupling is taken at the Z mass to be $\alpha_s(M_Z) \simeq 0.118$. The plots are only meant to give a rough estimate of the effects of NGLs in non-clustered as well as clustered final states.

where \tilde{R} is the jet-radius parameter used in `FastJet`¹⁸. Compared to eqs (2.3) and (2.4), $\tilde{R} = \cos^{-1}(1 - 2R_s)$. The exact numerical distributions $(1/\sigma_0)(d\sigma_e/dL)$, with $L = -\tilde{L} = \ln(\tau_{E_0})$, for the three colour channels, C_F^2 , $C_F C_A$ and $C_F T_R n_f$, have been obtained with 10^{11} events in the bin range $0 > L > -14$. We have used four values for the jet-radius: $R_s = 0.50$, $R_s = 0.30$, $R_s = 0.12$ and $R_s = 0.04$, with an energy veto $E_0 = 0.01 Q$. Standard deviations on individual bins range from $10^{-4}\%$ to $10^{-2}\%$.

We plot the difference between the numerical and analytical distributions at both LO and NLO,

$$r(L) = \frac{d\sigma_e}{\sigma_0 dL} - \frac{d\sigma_{r,2}}{\sigma_0 dL}, \quad (5.2)$$

where $d\sigma_{r,2}/\sigma_0 dL$ is given in eq. (B.6). Recall that at small values of the jet shape, τ_{E_0} , the finite remainder function $D_{\text{fin}}(\tau_{E_0})$ is vanishingly small and will thus be ignored. For the case where the jet shape is global ($R_s = 0.50$ and the threshold thrust reduces to thrust), we expect a full cancellation of singular terms and thus r should be a constant line corresponding to the NNLL coefficient (H_{21} in eq. (B.5)). For $R_s < 0.5$, the jet shape

¹⁸In `FastJet`'s manual \tilde{R} is allowed to go up to π . Since we are interested in two-jet events the jet size cannot be wider than a hemisphere. Thus we restrict \tilde{R} to be less than $\pi/2$.

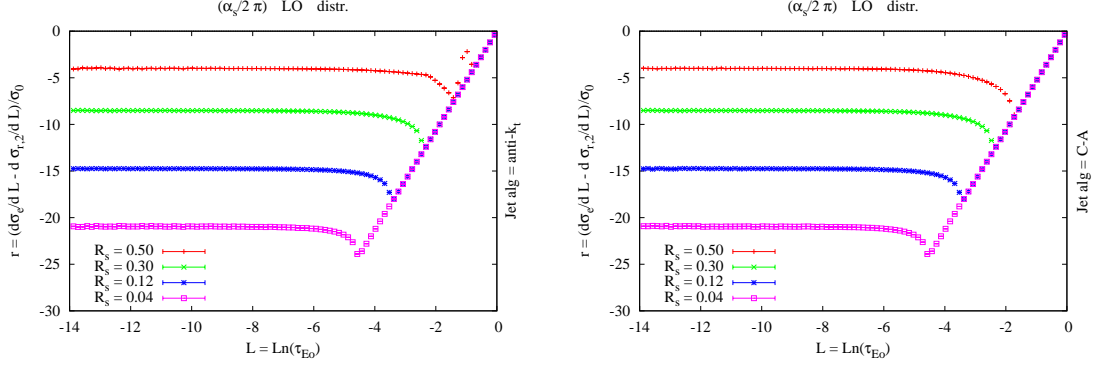


Figure 6: The difference between EVENT2 and τ_{E_0} LO distribution for various jet radii in both anti- k_t (left) and CA (right) algorithms.

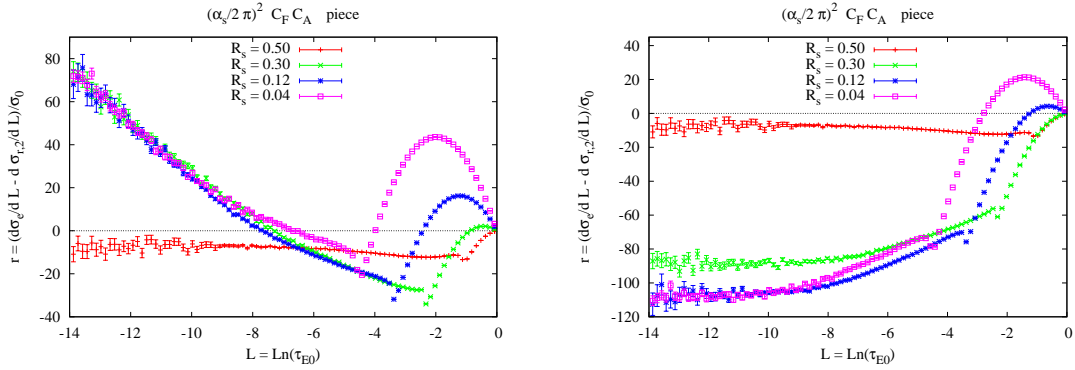


Figure 7: The $C_F C_A$ part of the difference between EVENT2 and (left) τ_{E_0} primary (global) distribution and (right) τ_{E_0} distribution including NGLs for various jet radii in anti- k_t algorithm.

is non-global and we expect r to have a slope if NGLs contribution is excluded. If our analytical calculations of the NGLs' coefficient, both for anti- k_t and C-A algorithms, are correct then upon adding the latter to H_{22} the slope should vanish and r becomes flat signalling a complete cancellation of terms up to NLL level. Similar behaviour should be seen with the CLs' coefficient C_2^P for the C-A algorithm case. Considering figs. 6 - 14, we make the following observations:

- At LO, the distribution is independent of the jet definition. From eq. (B.5) we have

$$H_{11} = -3 + 4L_{R_s} = -4, -8.51, -14.75, -20.95; \quad \text{for } R_s = 0.5, 0.3, 0.12, 0.04. \quad (5.3)$$

Compared to the numerical results shown in fig. 6 we see a complete agreement. The cut-off in fig. 6 is due to the fact that at LO $\tau_{E_0} < R_s/(1 + R_s)$ (eq. (2.10)).

- For the NLO distribution in the anti- k_t algorithm, fig. 7 (left) illustrates the existence of NGLs. The flatness of the $r(L)$ curve, in fig. 7 (right), at L below about

R_s	Jet alg	$C_F T_R n_f$ piece of		$C_F C_A$ piece of		C_F^2 piece of	
		H_{21}^{num}	H_{21}^{analyt}	H_{21}^{num}	H_{21}^{analyt}	H_{21}^{num}	H_{21}^{analyt}
0.50	anti- k_t	5.20 ± 0.14	5.00	-7.26 ± 0.22	-7.04	-12.40 ± 0.57	-12.68
	C-A	4.99 ± 0.19		-6.97 ± 0.11		-12.99 ± 0.67	
0.30	anti- k_t	13.92 ± 0.15	7.80	-88.35 ± 0.26	-11.45	62.73 ± 0.51	62.20
	C-A	11.24 ± 0.08		-48.46 ± 0.31		76.38 ± 0.50	
0.12	anti- k_t	15.75 ± 0.12	8.54	-106.80 ± 0.34	-8.89	384.04 ± 0.90	385.27
	C-A	13.65 ± 0.08		-51.46 ± 0.35		405.48 ± 0.57	
0.04	anti- k_t	12.86 ± 0.19	5.66	-107.67 ± 0.28	3.59	1017.93 ± 0.53	1022.43
	C-A	10.60 ± 0.23		-45.67 ± 0.23		1044.33 ± 1.24	

Table 1: H_{21} numerical vs analytical values for all three colour pieces. The numerical values were obtained through fitting the *flat* curve $r(\tilde{L})$ with the function (see eq. (B.7)) $H_{21}^{\text{num}} + e^{-\tilde{L}}(B + C e^{-\tilde{L}})$. The analytical values, H_{21}^{analyt} , are taken from eqs. (B.5) and (C.4) which only include the primary emission contribution with neither non-global nor clustering terms. $R_s = 0.50$ corresponds to the global case and we expect the analytical and numerical values to be the same.

-9 indicates a complete cancellation up to single log level. The C_F^2 and $C_F T_R n_f$ pieces are shown in fig. 8. In table 1 we provide both numerical and analytical, taken from SCET calculations (C.4), values of the NNLL coefficient, H_{21} , at the considered R_s values for the three colour channels. It is evident from the table that there are subleading R_s -dependent NGLs for both $C_F C_A$ and $C_F T_R n_f$ channels. Such logs have been analytically computed in [36] for the hemisphere jet mass. Our numerical results show that they are also present for finite-size jets¹⁹. The primary C_F^2 channel is free from such subleading NGLs as numerical and analytical values of H_{21} in the anti- k_t coincide.

Notice that while the x -axis in all figures shown in this section corresponds to $\ln(\tau_{E_0}) = \log(\tau_{E_0})$, i.e, the natural logarithm of the jet shape, that of [5] corresponds to the logarithm of base 10, $\log_{10}(\rho) \sim \log(\rho)/2$, $\rho \equiv \tau_{E_0}$, of the jet shape. Given this, fig. 7 above is equivalent to fig. 7 of [5]. Neither $C_F^2, C_F T_R n_f$ plots nor subleading NGLs were considered in [5].

- The asymptotic region, i.e, the region where large logs are expected to dominate over non-logarithmic contributions, corresponds to L less than about -9 (for figs. 7, C_F^2 piece in fig 8 and may even be less for the $C_F T_R n_f$ piece in fig. 8) and seems to decrease further as R_s becomes smaller. A similar effect is seen in the thrust distribution, fig. 9, where the numerical distribution has been obtained using the full definition (2.5).
- Considering the clustering case with C-A algorithm, figs. 10 and 11 illustrate the presence of CLs in the C_F^2 channel. Clearly, the addition of CLs makes the remainder r flat in the region $L \lesssim -9$. To strengthen this observation even more, we plot in

¹⁹as would be anticipated, since the finite-size jet mass is an extension to the hemisphere mass.

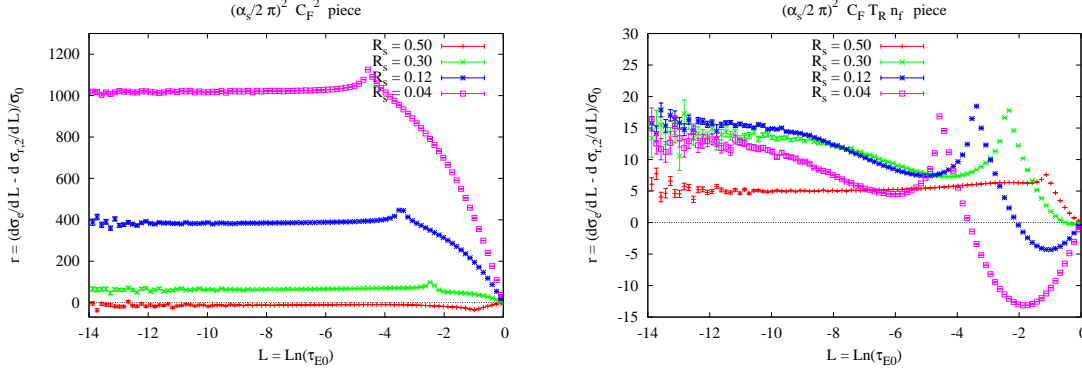


Figure 8: The (left) C_F^2 and (right) $C_F T_R n_f$ piece of the difference between `EVENT2` and τ_{E_0} distribution for various jet radii in the anti- k_t algorithm.

fig. 12 the difference between `EVENT2` distributions in anti- k_t and C-A algorithms, $(d\sigma_e^{\text{anti-}k_t}/dL - d\sigma_e^{\text{C-A}}/dL)/\sigma_0$, for all colour pieces. The slopes for the C_F^2 and $C_F C_A$ indicate that an NLL positive R_s -dependent term, and possibly an NNLL term as well, have been induced by clustering. This is confirmed in table 1. Moreover, the fact that the difference between the latter distributions in the $C_F T_R n_f$ piece is non-vanishing implies an NNLL impact of clustering.

Furthermore, we note from fig. 11 that C_2^P seems to slightly vary with the jet-radius parameter R_s . This can be seen for large values of R_s ($R_s = 0.3$) where our small angles approximation (3.24) is not expected to apply.

- Similar analysis to those carried in the anti- k_t algorithm apply to the $C_F C_A$ piece of the τ_{E_0} distribution in the C-A algorithm. Including the NGLs makes the $r(L)$ curve looks convincingly flat in the region $L \lesssim -9$, particularly for smaller values of R_s , as shown in fig. 13. Recall that we have used the small R_s limit in carrying out the computation of $S_2^{\text{C-A}}$, eq. (3.32). Our findings agree with those reported in [5] for jet-radii up to $R_s \sim 0.3$ ($R \sim 1$).

For completeness, the $C_F T_R n_f$ piece of the $r(L)$ in the C-A algorithm is depicted in fig. 14. As shown in table 1, clustering requirement again reduces the impact of the subleading NGLs in both $C_F C_A$ and $C_F T_R n_f$ channels.

In summary, we have confirmed through explicit comparison to exact numerical distributions the existence of large NGLs and large CLs for the τ_{E_0} distribution at NLL and beyond. In light of these findings, the surprising cancellation between primary-only analytical distribution and `EVENT2` presented in [4] v1 may be explained as follows. While each colour part (C_F^2 , $C_F C_A$ and $C_F T_R n_f$) separately does not agree with `EVENT2`, as shown in figs. 10, 11, 13 and 14, their sum seems to agree with `EVENT2` (recall that in of [4] v1 only the sum of the three colour factors is plotted against `EVENT2`). Such an unexpected agreement can arise from the following possible sources:

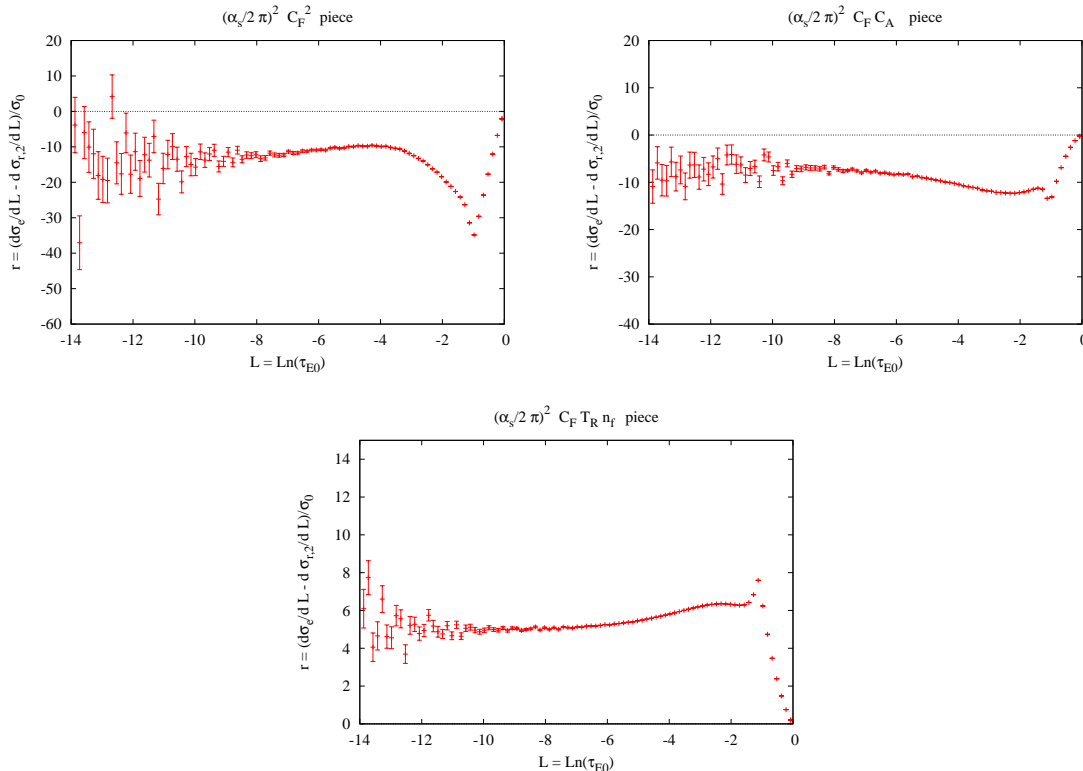


Figure 9: The various colour pieces of the difference between **EVENT2** and thrust distribution using the full definition (2.5). The pQCD resummed analytical expression for thrust distribution can be found in, for example, [11].

- The $\ln(\tau_{E0})$ region considered in [4] v1 does not correspond to the asymptotic region where large logs are expected to dominate over non-logarithmic terms. Thus the agreement shown in plot 1 of [4] v1 does not convey any message and all one can say is that the non-logarithmic terms in the range $[-9, 0]$ happen to cancel out (see fig 15).
- NGLs are significantly reduced in the C – A algorithm especially for a jet radius $R_s = 0.3$ (which is the one considered in [4] v1), as clearly seen in figs. 4 and 13 (left). For smaller jet radii, there is a clear disagreement between the result of [4] v1 and **EVENT2** as shown in fig. 15

We have also shown that clustering the final state partons with the C–A algorithm yielded a significant reduction in NGLs impact, at NLL and beyond, albeit inducing large CLs, at NLL and beyond, in the primary emission sector.

6 Conclusion

The jet mass with a jet veto, or simply the threshold thrust, is an example of a wider class of non-global observables. These have the characteristic of being sensitive to radiation into restricted regions of phase space, or sensitive to radiation into the whole phase space

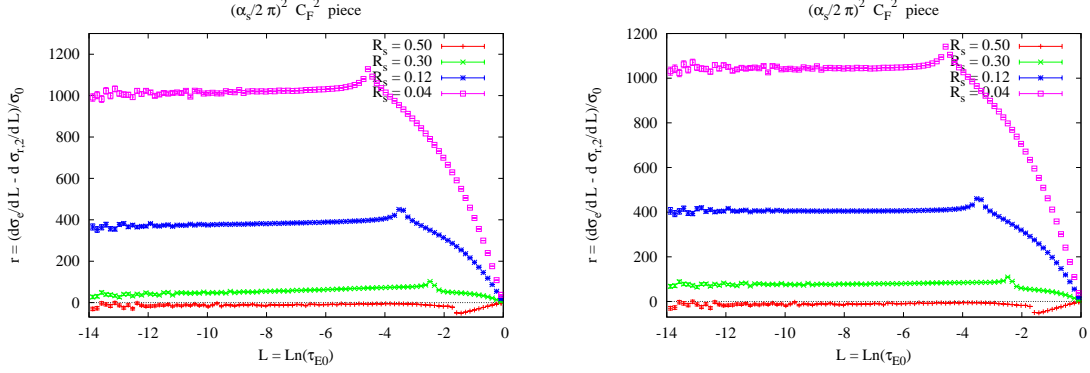


Figure 10: The C_F^2 part of the difference between **EVENT2** and (left) τ_{E_0} primary (global) distribution and (right) τ_{E_0} distribution including CLs for various jet radii in the C–A algorithm.

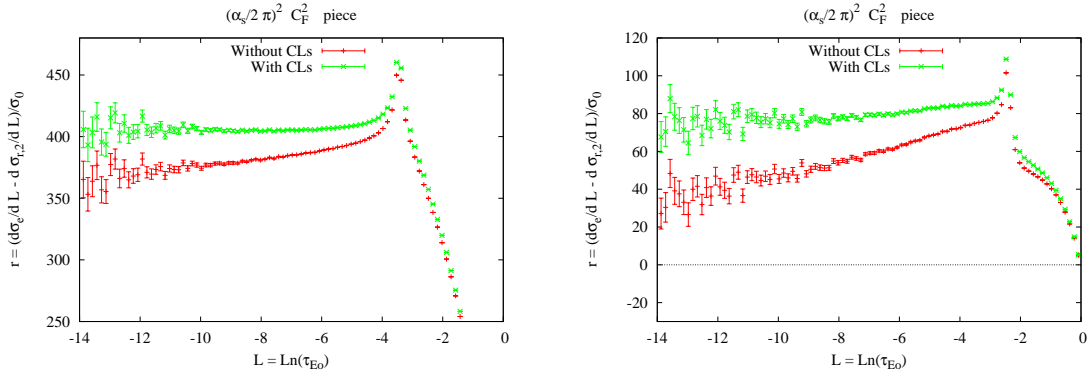


Figure 11: Zoomed–in plots for the C_F^2 part of the difference between **EVENT2** and analytical τ_{E_0} distribution with and without CLs for (left) $R_s = 0.12$ and (right) $R_s = 0.3$ in the C–A algorithm.

but differently in different regions. For such observables the universal Sudakov form factor fails to reproduce the full logarithmic structure even at NLL accuracy. New contributions that are dependent on various variables such as the jet size and jet definition appear at this logarithmic level. In this paper, we have elaborated on these very contributions for the aforementioned observable.

Considering secondary emissions, we have computed the full analytical expression of the first term, S_2 , in a series of missing large logs, namely NGLs. The coefficient depends, as anticipated, on the jet size and saturates at its maximum in the limit where the latter, i.e, jet size, vanishes. This saturation value was used in [3] as an approximation to the full value in the small R_s limit. It turns out that the approximation is valid for quite a wide range of R_s . The formula for S_2 has been checked against full exact numerical result obtained by the program **EVENT2**. The difference between the analytical and numerical differential distributions was shown to be asymptotically flat signalling a complete cancellation of singular terms up to NLL level. This has all been done for final states defined in the cone–like anti– k_t jet algorithm.

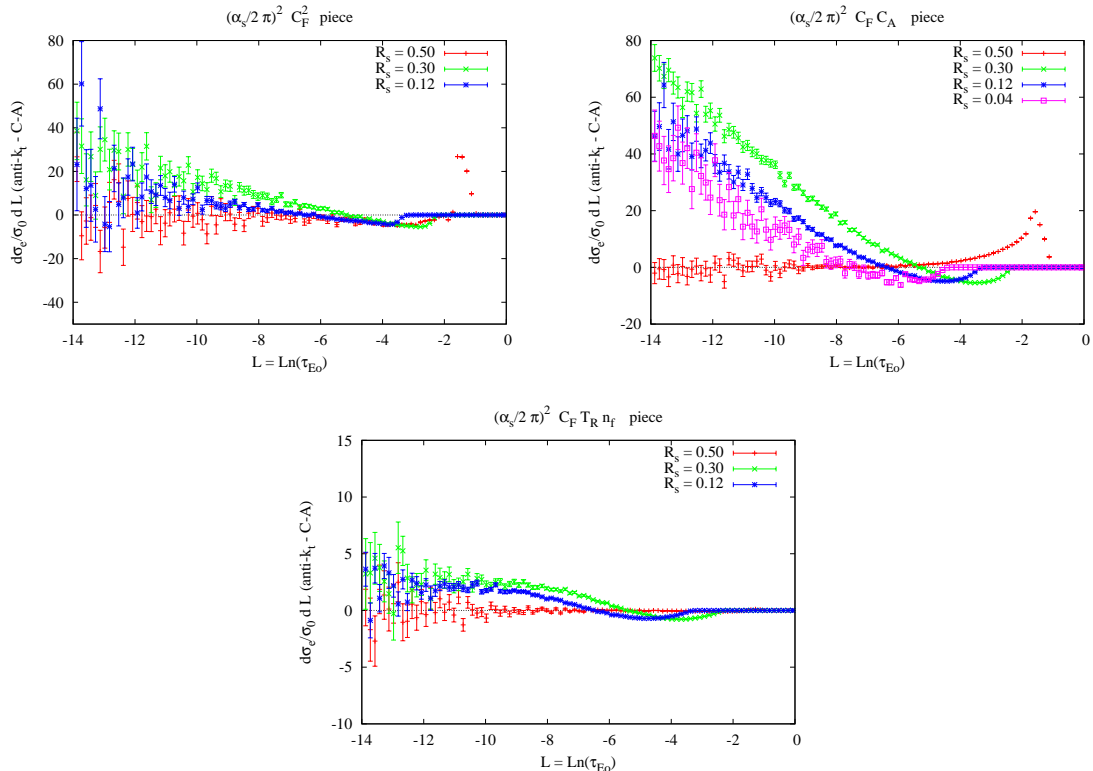


Figure 12: Plots of the three colour pieces of the difference between two `EVENT2` distributions corresponding to anti- k_t and C-A algorithms for various jet radii. We only show C_F^2 and $C_F T_R n_f$ results at three values of the jet-radius due to large errors in these colour channels.

To illustrate the dependence of NLL on the jet definition, we have investigated the effects of applying the C-A algorithm on e^+e^- final states. The impact of soft partons clustering is two-fold. On one side, it reduces the size of NGLs through shrinking the phase space region where the latter dominantly come from. i.e, the region where the emitter and emitted soft partons are just in and just out of the jet. On the other side, it gives rise to new NLL logarithmic contributions, CLs, in the primary emission sector. In the small jet-radius limit, the corresponding coefficient at second order has been shown, through comparison to `EVENT2`, to be independent of R_s .

Furthermore, our numerical analyses with `EVENT2` have shown that the asymptotic region where the said large logs, in both anti- k_t and C-A jet algorithms, dominate corresponds to $L \lesssim -9$ and decreases for smaller values of the jet-radius. As a by-product, we have found that there are subleading NGLs in both $C_F C_A$ and $C_F T_R n_f$ pieces as well as subleading CLs in the C_F^2 piece of the τ_{E_0} distribution. Clustering impact on NGLs has been observed to extend to NNLL level too. Regarding NGLs in $C_F C_A$ channel in both jet algorithms, our findings serve as a confirmation of the corresponding calculations performed within SCET in [5].

Based on our rough approximation to NLL resummation, which is exponentiating the fixed-order result for both NGLs and CLs, it has been shown that it may be possible to completely eliminate the non-global correction to the primary Sudakov form factor

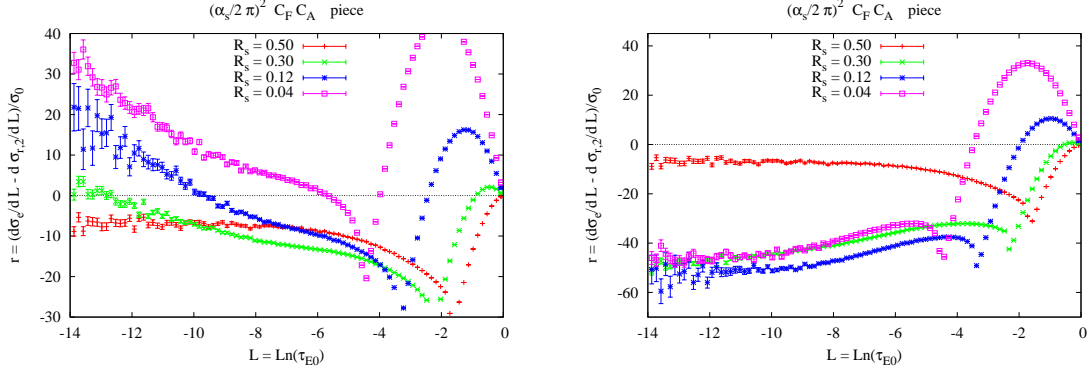


Figure 13: The $C_F C_A$ part of the difference between EVENT2 and (left) τ_{E_0} primary (global) distribution and (right) τ_{E_0} distribution including NGLs for various jet radii in the C–A algorithm.

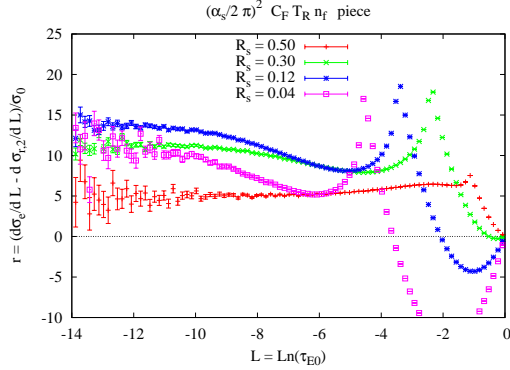


Figure 14: The $C_F T_R n_f$ piece of the difference between EVENT2 and τ_{E_0} distribution for various jet radii in C – A algorithm.

at all-orders for events where final states clustering is applied. This elimination can be achieved by tuning the jet-radius parameter, R_s , of the jet algorithm as well as the jet veto E_0 . If such *optimal* values of R_s and E_0 are of practical significance, that is $R \sim 0.4$ or so and $E_0 \gg \Lambda_{\text{QCD}}$, then the single-gluon exponentiation should be sufficient in describing the experimental data. A concrete answer of whether such optimal values exist can only be established once an all-orders resummation of primary, NGLs and CLs is performed. We postpone this investigation to future publications.

As mentioned earlier in sec. 3 and shown in [3], the inclusive k_t jet algorithm behaves in an identical way to C–A algorithm with regard to the threshold thrust distribution. It would be interesting to conduct similar studies for events defined in IRC cone algorithms such as the SISCone. In principle, one expects to see analogous effects not only for the threshold thrust but for all shape variables that are of non-global nature. Moreover, we reserve the extension of the findings of this paper to hadron–hadron collisions to future work. Apart from complications due to coloured initial state, we expect the gross features of this paper to apply.

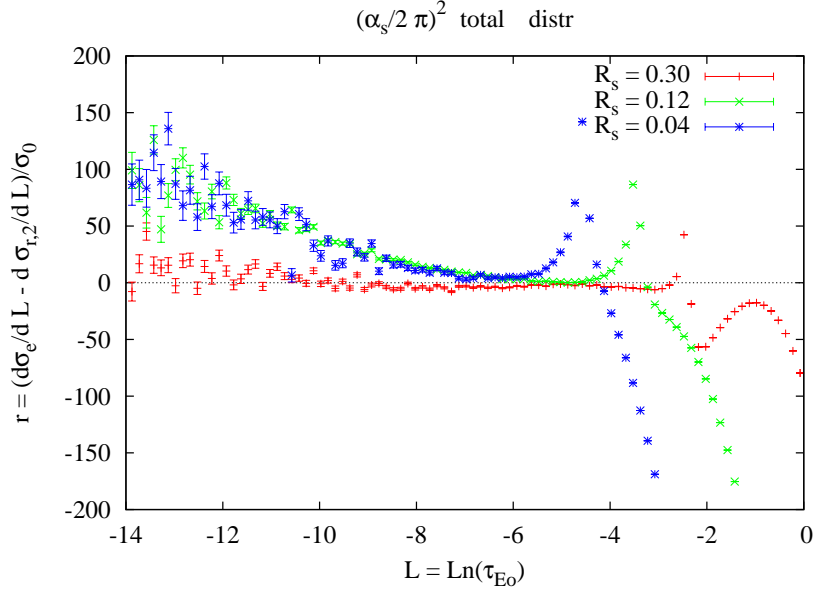


Figure 15: Difference between the sum of the three colours and EVENT2 for various jet radii.

Acknowledgement

I am indebted to M. Dasgupta, S. Marzani and A. Banfi for collaboration on related work and helpful discussions on the current paper. I would like to thank M. Seymour for his generous help and useful feedback.

A Derivation of LO distribution

In the present section we outline the derivation of the full logarithmic part of the LO τ_{E_0} integrated distribution (2.10). For the emission of a single gluon, i.e. $e^+e^- \rightarrow q\bar{q}g$, we define the kinematic variables, $x_i = 2p_i \cdot Q/Q^2 = 2E_i/Q$ and $y_{ij} = 2p_i \cdot p_j/Q^2 = 1 - x_k$ where $i, j, k = 1(q), 2(\bar{q}), 3(g)$. The $\mathcal{O}(\alpha_s)$ matrix-element squared can be computed by considering two Feynman graphs corresponding to real emission of the gluon g off the two hard legs q, \bar{q} . Applying the appropriate QCD Feynman rules and supplementing the three-body phase space factor, the corresponding differential distribution is given by

$$\frac{d^2\sigma^{(1)}}{\sigma dx_1 dx_2} = \frac{C_F \alpha_s}{2\pi} \frac{x_1^2 + x_2^2}{(1-x_1)(1-x_2)}, \quad (\text{A.1})$$

where σ is the total hadronic cross-section. Up to $\mathcal{O}(\alpha_s^2)$, it is given in terms of the Born cross-section, σ_0 , by the relation [41]

$$\frac{\sigma}{\sigma_0} = 1 + \frac{\alpha_s}{2\pi} \left[\frac{3C_F}{2} \right] + \left(\frac{\alpha_s}{2\pi} \right)^2 K_2 + \mathcal{O}(\alpha_s^3). \quad (\text{A.2})$$

with

$$K_2 = -C_F^2 \frac{3}{8} + C_F C_A \left(\frac{123}{8} - 11\zeta_3 \right) + C_F T_R n_f \left(-\frac{11}{2} + 4\zeta_3 \right). \quad (\text{A.3})$$

The integration region, which is originally $1 \geq x_1, x_2 \geq 0$ and $x_1 + x_2 \geq 1$ and which leads to divergences, gets modified by introducing the jet shape variable. For three partons in the final state, τ_{E_0} is zero unless two partons are clustered together. Therefore τ_{E_0} is non-vanishing only in two-jet events. For the latter events, there are six ways of ordering the energy fractions x_i corresponding to six regions of phase space that needs to be integrated over. Due to $x_1 \leftrightarrow x_2$ symmetry of the matrix-element (A.1), one can only consider three regions and multiply the result by a factor of 2. These regions correspond to; $x_1 > x_2 > x_3, x_1 > x_3 > x_2$ and $x_3 > x_1 > x_2$. The threshold thrust is then given by

$$\begin{aligned} \tau_{E_0} = & (1 - x_1)\Theta(x_1 - x_2, x_2 - x_3)\Theta(2R_s - 1 + \cos\theta_{23}) + \\ & + (1 - x_1)\Theta(x_1 - x_3, x_3 - x_2)\Theta(2R_s - 1 + \cos\theta_{23}) + \\ & + (1 - x_3)\Theta(x_3 - x_1, x_1 - x_2)\Theta(2R_s - 1 + \cos\theta_{12}), \end{aligned} \quad (\text{A.4})$$

where $\Theta(a-b, b-c) = \Theta(a-b)\Theta(b-c)$. To obtain the full logarithmic contribution it is sufficient to only consider regions where the gluon is the softest parton ($x_3 = \min(x_i)$). Other regions, last term in RHS of eq. (A.4), only contributes non-logarithmically. Adding up real and virtual contributions, in (2.8), one is only left with the virtual corrections in the range $\Theta(1 - x_1 - \tau_{E_0})$. The corresponding angular function in (A.4) may be written in terms of the energy fractions as,

$$1 - \cos\theta_{23} = \frac{2(1 - x_1)}{x_2 x_3} \approx \frac{2(1 - x_1)}{x_3}, \quad (\text{A.5})$$

where the last approximation follows from the fact that the gluon is the softest, $x_1, x_2 \gg x_3$. Hence the two-jet contribution to the first order shape fraction $\Sigma^{(1)}$ is given by

$$\Sigma^{(1)}(\tau_{E_0}, E_0) = -\frac{C_F \alpha_s}{2\pi} \int_{1-R_s(1-\tau_{E_0})}^{1-\tau_{E_0}} dx_2 \int_{1+\tau_{E_0}+x_2}^{\frac{x_2-1+R_s(2-x_2)}{R_s}} dx_1 \frac{x_1^2 + x_2^2}{(1-x_1)(1-x_2)} \Theta\left(\frac{R_s}{1+R_s} - \tau_{E_0}\right) \quad (\text{A.6})$$

In case of events with three-jets in the final state, the energy of the softest jet is vetoed to be less than E_0 . The corresponding phase space constraint, left after real-virtual mis-cancellation, on the differential cross-section (A.1) reads

$$-\Theta\left(x_3 - \frac{2E_0}{Q}\right) \Theta\left(\frac{1-x_1}{x_3} - R_s\right) \Theta\left(1 - R_s - \frac{1-x_1}{x_3}\right). \quad (\text{A.7})$$

Noting that $x_1 + x_2 + x_3 = 2$, one can obtain the corresponding integration limits on x_1 and x_2 . Adding up the result of the latter integration with that of eq. (A.6) and making use of the following dilogarithm identities [42]

$$\begin{aligned} \text{Li}_2(x) + \text{Li}_2(1-x) &= \frac{\pi^2}{6} - \ln(x) \ln(1-x), \\ \text{Li}_2(x) + \text{Li}_2\left(\frac{1}{x}\right) &= \frac{\pi^2}{3} - \frac{1}{2} \ln^2(x). \end{aligned} \quad (\text{A.8})$$

one obtains eq. (2.10).

B G_{nm} coefficients

The resultant coefficients from the expansion of the exponent in the resummed integrated distribution, eq. (4.5), are

$$\begin{aligned}
G_{12} &= -2C_F, \\
G_{11} &= C_F(3 - 4L_{R_s}), \\
G_{10} &= C_F \left[-4L_{R_s}L_{E_0} + \frac{\bar{f}_0(R_s)}{2} \right], \\
G_{23} &= C_F \left(\frac{4}{3}T_R n_f - \frac{11}{3}C_A \right), \\
G_{22} &= -\frac{4\pi^2}{3}C_F^2 + C_F C_A \left(\frac{\pi^2}{3} - S_0(R_s) - \frac{169}{36} - \frac{22}{3}L_{R_s} \right) + C_F T_R n_f \left(\frac{11}{9} + \frac{8}{3}L_{R_s} \right), \\
G_{21} &= -C_F^2 \frac{8\pi^2}{3}L_{R_s} - C_F C_A \left[2S_0(R_s)L_{E_0} - \left(\frac{2\pi^2}{3} - 2S_0(R_s) - \frac{134}{9} - \frac{11}{3}L_{R_s} \right) L_{R_s} \right] + \\
&\quad + C_F T_R n_f \left(\frac{4}{3}L_{R_s} + \frac{40}{9} \right) L_{R_s}. \tag{B.1}
\end{aligned}$$

where $L_{R_s} = \ln(R_s/(1 - R_s))$ and $L_{E_0} = \ln(2E_0/Q)$. The factor $\bar{f}_0(R_s)$ only captures the first term of f_0 given in eq. (2.11). We simply replace $\bar{f}_0 \mapsto f_0$ when comparing to the numerical distribution. Moreover, we have introduced, for shorthand, the function $S_0(R_s)$ given by (cf. eq. (3.12)),

$$S_2 = -C_F C_A S_0(R_s). \tag{B.2}$$

The one-loop constant is given by, eq. (2.10),

$$C_1 = C_F \left(-1 + \frac{\pi^2}{3} \right), \tag{B.3}$$

Expanding the total resummed distribution in eq. (4.5) to $\mathcal{O}(\alpha_s^2)$ and up to NLL we have

$$\begin{aligned}
\Sigma_{r,2}(\tilde{L}) &= 1 + \left(\frac{\alpha_s}{2\pi} \right) \left(H_{12}\tilde{L}^2 + H_{11}\tilde{L} + H_{10} \right) + \left(\frac{\alpha_s}{2\pi} \right)^2 \left(H_{24}\tilde{L}^4 + H_{23}\tilde{L}^3 + H_{22}\tilde{L}^2 + \right. \\
&\quad \left. + H_{21}\tilde{L} + H_{20} \right), \tag{B.4}
\end{aligned}$$

where (recall that $\tilde{L} = \ln(1/\tau_{E_0}) \Rightarrow \tau_{E_0} = e^{-\tilde{L}}$)

$$\begin{aligned}
D_{\text{fin}}(e^{-\tilde{L}}) &= \left(\frac{\alpha_s}{2\pi}\right) d_1(e^{-\tilde{L}}) + \left(\frac{\alpha_s}{2\pi}\right)^2 d_2(e^{-\tilde{L}}), \\
H_{12} &= G_{12}, \\
H_{11} &= G_{11}, \\
H_{10} &= G_{10} + C_1 + d_1(\tau_{E_0}), \\
H_{24} &= \frac{1}{2}G_{12}^2, \\
H_{23} &= G_{23} + G_{12}G_{11}, \\
H_{22} &= G_{22} + (G_{10} + C_1)G_{12} + \frac{1}{2}G_{11}^2, \\
H_{21} &= G_{21} + (G_{10} + C_1)G_{11}, \\
H_{20} &= G_{20} + \frac{1}{2}G_{10}^2 + C_1G_{10} + C_2 + d_2(\tau_{E_0}).
\end{aligned} \tag{B.5}$$

Differentiating (B.4) w.r.t. \tilde{L} , the NLO differential distribution reads

$$\frac{d\Sigma_{r,2}}{d\tilde{L}} = \frac{1}{\sigma_0} \frac{d\sigma_{r,2}}{d\tilde{L}} = \delta(\tilde{L}) D_\delta + \left(\frac{\alpha_s}{2\pi}\right) D_A(\tilde{L}) + \left(\frac{\alpha_s}{2\pi}\right)^2 D_B(\tilde{L}), \tag{B.6}$$

where the singular (logarithmic) terms are given by

$$\begin{aligned}
D_\delta &= 1 + \left(\frac{\alpha_s}{2\pi}\right) [G_{10} + C_1] + \left(\frac{\alpha_s}{2\pi}\right)^2 \left[G_{20} + \frac{1}{2}G_{10}^2 + C_1G_{10} + C_2 \right], \\
D_A(\tilde{L}) &= 2H_{12}\tilde{L} + H_{11} + \frac{d}{d\tilde{L}} d_1(e^{-\tilde{L}}), \\
D_B(\tilde{L}) &= 4H_{24}\tilde{L}^3 + 3H_{23}\tilde{L}^2 + 2H_{22}\tilde{L} + H_{21} + \frac{d}{d\tilde{L}} d_2(e^{-\tilde{L}}).
\end{aligned} \tag{B.7}$$

C Threshold thrust distribution in SCET

The resummation of the threshold thrust in SCET is presented in the current section for comparison with pQCD. We shall only present the final form of the resummed result taken from Refs. [4, 24, 27]. For a full derivation and more in depth discussion one should consult the latter references. The only task we have performed here is the expansion of the full resummed distribution to $\mathcal{O}(\alpha_s^2)$.

C.1 Resummation

The general formula of the resummed distribution for the threshold thrust is given by [4, 27]

$$\begin{aligned} \frac{d\Sigma^{\text{SCET}}(\tau_{E_0}, R)}{d\tau_{E_0}} &= \frac{d\sigma^{\text{SCET}}}{\sigma_0 d\tau_{E_0}} = \exp[4S(\mu_h, \mu_j) + 4S(\mu_s, \mu_j) - 4A_H(\mu_h, \mu_s) + 4A_J(\mu_j, \mu_s)] \\ &\times \left(\frac{R_s}{1-R_s}\right)^{-2A_\Gamma(\mu_\omega, \mu_s)} \left(\frac{Q^2}{\mu_h^2}\right)^{-2A_\Gamma(\mu_h, \mu_j)} H(Q^2, \mu_h) S_R^{\text{out}}(\omega, \mu_\omega) \\ &\times \left[\tilde{j}\left(\ln\frac{\mu_s Q}{\mu_j^2} + \partial_\eta, \mu_j\right)\right]^2 \tilde{s}_{\tau_{E_0}}^{\text{in}}(\partial_\eta, \mu_s) \frac{1}{\tau_{E_0}} \left(\frac{\tau_{E_0} Q}{\mu_s}\right)^\eta \frac{e^{-\gamma_E \eta}}{\Gamma(\eta)}. \end{aligned} \quad (\text{C.1})$$

See [4, 27] for full notation. In order to compute the fixed-order expansion of (C.1) up to $\mathcal{O}(\alpha_s^2)$, all scales should be set equal ($\mu_h = \mu_j = \mu_s = Q$). In this limit, the evolution factors S , A_J and A_H vanish. The differentiation w.r.t. η is carried out using the explicit form of \tilde{j} and $\tilde{s}_{\tau_{E_0}}^{\text{in}}$. The final result of the integrated distribution may be cast in the generic form (4.5) with the constants and coefficients of the logs given by

$$C_1 = C_F \left(-1 + \frac{\pi^2}{3}\right), \quad (\text{C.2})$$

$$\begin{aligned} C_2 &= C_F^2 \left(1 - \frac{3\pi^2}{8} + \frac{\pi^4}{72} - 6\zeta(3)\right) + C_F C_A \left(\frac{493}{324} + \frac{85\pi^2}{24} - \frac{73\pi^4}{360} + \frac{283\zeta(3)}{18}\right) + \\ &+ C_F T_R n_f \left(\frac{7}{81} - \frac{7\pi^2}{6} - \frac{22\zeta(3)}{9}\right) + C_2^{\text{in}} + C_2^{\text{out}}, \end{aligned} \quad (\text{C.3})$$

and

$$\begin{aligned} G_{12} &= -2C_F, \\ G_{11} &= -C_F(3 - 4L_{R_s}), \\ G_{10} &= C_F \left(-4L_{R_s} L_{E_0} + \frac{f_0(R_s)}{2}\right), \\ G_{23} &= C_F \left(\frac{11}{3}C_A - \frac{4}{3}T_R n_f\right), \\ G_{22} &= -\frac{4\pi^2}{3}C_F^2 + C_F C_A \left(\frac{\pi^2}{3} - \frac{169}{36} - \frac{22}{3}L_{R_s}\right) + C_F T_R n_f \left(\frac{11}{9} + \frac{8}{3}L_{R_s}\right), \\ G_{21} &= C_F^2 \left[-\frac{3}{4} - \pi^2 + 4\zeta(3) + \frac{8\pi^2}{3}L_{R_s}\right] + \\ &+ C_F C_A \left[-\frac{57}{4} + 6\zeta(3) - \left(\frac{2\pi^2}{3} - \frac{134}{9} - \frac{11}{3}L_{R_s}\right)L_{R_s}\right] + \\ &+ C_F T_R n_f \left[5 - \left(\frac{4}{3}L_{R_s} + \frac{40}{9}\right)L_{R_s}\right], \end{aligned}$$

$$\begin{aligned}
G_{20} &= C_F^2 \left[-\frac{f_0^2}{8} + (2\pi^2 - 16\zeta(3)) L_{R_s} - \left(\frac{11\pi^2}{6} + \frac{f_0}{2} \right) L_{R_s}^2 - L_{R_s}^2 \right] + \\
&+ C_F C_A \left[\frac{11\pi^2}{9} L_{R_s} - \frac{11}{6} L_{R_s} L_{E_0}^2 - L_{E_0} \left(\frac{11f_0}{12} + \left[\frac{134}{9} - \frac{2\pi^2}{3} \right] L_{R_s} + \frac{11}{6} L_{R_s}^2 \right) \right] + \\
&+ C_F T_R n_f \left[-\frac{4\pi^2}{9} L_{R_s} + \frac{2}{3} L_{R_s} L_{E_0}^2 + L_{E_0} \left(\frac{f_0(R_s)}{3} + \frac{40}{9} L_{R_s} + \frac{2}{3} L_{R_s}^2 \right) \right]. \quad (\text{C.4})
\end{aligned}$$

Considering primary emission, the only missing piece in the distribution is the two-loop constants in the soft function, namely C_2^{in} and C_2^{out} .

References

- [1] S. D. Ellis, A. Hornig, C. Lee, C. K. Vermilion, and J. R. Walsh *Phys. Lett.* **B689** (2010) 82–89, [[arXiv:0912.0262](#)].
- [2] S. D. Ellis, C. K. Vermilion, J. R. Walsh, A. Hornig, and C. Lee *JHEP* **11** (2010) 101, [[arXiv:1001.0014](#)].
- [3] A. Banfi, M. Dasgupta, K. Khelifa-Kerfa, and S. Marzani *JHEP* **08** (2010) 064, [[arXiv:1004.3483](#)].
- [4] R. Kelley, M. D. Schwartz, and H. X. Zhu [arXiv:1102.0561](#).
- [5] A. Hornig, C. Lee, J. R. Walsh, and S. Zuberi [arXiv:1110.0004](#).
- [6] H.-n. Li, Z. Li, and C.-P. Yuan *Phys.Rev.Lett.* **107** (2011) 152001, [[arXiv:1107.4535](#)].
- [7] M. Dasgupta and G. P. Salam *J. Phys.* **G30** (2004) R143, [[hep-ph/0312283](#)].
- [8] M. Beneke *Phys. Rept.* **317** (1999) 1–142, [[hep-ph/9807443](#)].
- [9] B. Webber [hep-ph/9411384](#).
- [10] M. Beneke and V. M. Braun [hep-ph/0010208](#).
- [11] R. K. Ellis, W. J. Stirling, and B. R. Webber, *QCD and Collider Physics*. Cambridge monographs on particle physics, nuclear physics and cosmology. Cambridge University Press, 1996.
- [12] A. Abdesselam *et al.* *Eur. Phys. J.* **C71** (2011) 1661, [[arXiv:1012.5412](#)].
- [13] M. Dasgupta and G. P. Salam *Phys. Lett.* **B512** (2001) 323–330, [[hep-ph/0104277](#)].
- [14] S. Catani, L. Trentadue, G. Turnock, and B. R. Webber *Nucl. Phys.* **B407** (1993) 3–42.
- [15] A. Banfi, G. P. Salam, and G. Zanderighi *JHEP* **01** (2002) 018, [[hep-ph/0112156](#)].

- [16] A. Banfi, G. P. Salam, and G. Zanderighi *JHEP* **1006** (2010) 038, [[arXiv:1001.4082](#)].
- [17] D. de Florian and M. Grazzini *Nucl.Phys.* **B704** (2005) 387–403, [[hep-ph/0407241](#)].
- [18] A. Gehrmann-De Ridder, T. Gehrmann, and E. W. N. Glover *JHEP* **09** (2005) 056, [[hep-ph/0505111](#)].
A. Gehrmann-De Ridder, T. Gehrmann, E. W. N. Glover, and G. Heinrich *JHEP* **12** (2007) 094, [[arXiv:0711.4711](#)].
- [19] P. F. Monni, T. Gehrmann, and G. Luisoni *JHEP* **08** (2011) 010, [[arXiv:1105.4560](#)].
- [20] C. W. Bauer, S. Fleming, D. Pirjol, and I. W. Stewart *Phys. Rev.* **D63** (2001) 114020, [[hep-ph/0011336](#)].
C. W. Bauer, D. Pirjol, and I. W. Stewart *Phys. Rev.* **D65** (2002) 054022, [[hep-ph/0109045](#)].
- [21] Y.-T. Chien and M. D. Schwartz *JHEP* **08** (2010) 058, [[arXiv:1005.1644](#)].
R. Abbate, M. Fickinger, A. Hoang, V. Mateu, and I. W. Stewart *PoS RADCOR2009* (2010) 040, [[arXiv:1004.4894](#)].
- [22] M. Cacciari and G. P. Salam *Phys. Lett.* **B641** (2006) 57–61, [[hep-ph/0512210](#)].
- [23] M. Cacciari, G. P. Salam, and G. Soyez *JHEP* **04** (2008) 063, [[arXiv:0802.1189](#)].
- [24] R. Kelley and M. D. Schwartz *Phys. Rev.* **D83** (2011) 033001, [[arXiv:1008.4355](#)].
- [25] S. D. Ellis and D. E. Soper *Phys. Rev.* **D48** (1993) 3160–3166, [[hep-ph/9305266](#)].
- [26] S. Catani and M. H. Seymour *Phys. Lett.* **B378** (1996) 287–301, [[hep-ph/9602277](#)].
- [27] T. Becher and M. D. Schwartz *JHEP* **07** (2008) 034, [[arXiv:0803.0342](#)].
- [28] A. Gehrmann-De Ridder, T. Gehrmann, E. W. N. Glover, and G. Heinrich *Phys. Rev. Lett.* **99** (2007) 132002, [[arXiv:0707.1285](#)].
- [29] G. Oderda and G. F. Sterman *Phys. Rev. Lett.* **81** (1998) 3591–3594, [[hep-ph/9806530](#)].
- [30] M. Dasgupta and G. P. Salam *JHEP* **03** (2002) 017, [[hep-ph/0203009](#)].
- [31] R. B. Appleby and M. H. Seymour *JHEP* **12** (2002) 063, [[hep-ph/0211426](#)].
- [32] A. Banfi and M. Dasgupta *Phys. Lett.* **B628** (2005) 49–56, [[hep-ph/0508159](#)].
- [33] J. C. Collins, D. E. Soper, and G. F. Sterman *Nucl. Phys.* **B250** (1985) 199.
- [34] R. Bonciani, S. Catani, M. L. Mangano, and P. Nason *Phys. Lett.* **B575** (2003) 268–278, [[hep-ph/0307035](#)].

- [35] A. Banfi, G. Marchesini, and G. Smye *JHEP* **08** (2002) 006, [[hep-ph/0206076](#)].
- [36] R. Kelley, M. D. Schwartz, R. M. Schabinger, and H. X. Zhu *Phys. Rev.* **D84** (2011) 045022, [[arXiv:1105.3676](#)].
- [37] A. Hornig, C. Lee, I. W. Stewart, J. R. Walsh, and S. Zuberi *JHEP* **08** (2011) 054, [[arXiv:1105.4628](#)].
- [38] Y. Delenda, R. Appleby, M. Dasgupta, and A. Banfi *JHEP* **0612** (2006) 044, [[hep-ph/0610242](#)].
- [39] M. Cacciari, G. P. Salam, and G. Soyez [arXiv:1111.6097](#).
- [40] G. P. Salam and G. Soyez *JHEP* **05** (2007) 086, [[arXiv:0704.0292](#)].
- [41] T. Appelquist and H. Georgi *Phys. Rev.* **D8** (1973) 4000–4002.
- [42] <http://functions.wolfram.com/ZetaFunctionsandPolylogarithms/PolyLog2>.